On Fibre Suspension Flow Modelling: Mechanical Fibre Flocculation and Fibre Orientation

by

Marko Hyensjö

April 2005
Licentiate Thesis from
Royal Institute of Technology
Department of Mechanics
SE-100 44 Stockholm, Sweden

Akademisk avhandling som med tillstånd av Kungliga Tekniska Högskolan i Stockholm framlägges till offentlig granskning för avläggande av teknologie licentiatexamen måndagen den 11:e april 2005 kl 10.15 i Sal L1, Kungliga Tekniska Högskolan, Drottning Kristinas väg 30, Stockholm.

Universitetsservice US AB, Stockholm 2005

On Fibre Suspension Flow Modelling: Mechanical Fibre Flocculation and Fibre Orientation

Marko Hyensjö 2005
Department of Mechanics, Royal Institute of Technology
SE-100 44 Stockholm, Sweden.

Abstract

In this work the main target is to study numerically the mechanical fibre flocculation and fibre orientation for a cellulose fibre suspension. The aim is specially to develop fibre flocculation and fibre orientation models for turbulent flows in complex geometries, i.e. typical to be found in paper machine equipment. Furthermore the aim is to study the dilute consistency regime, i.e. <1%, which is expected in papermaking.

Different mechanical flocculation models for turbulent one phase flow is tested for various geometries, i.e. a sudden pipe expansion and a planar contraction. The sudden pipe expansion is studied for various flow rates and with fixed step size and fibre properties. For the planar contraction two flocculation models in literature are evaluated. Various parameters such flow rate, fibre properties, inlet turbulence quantities are explored.

The fibre floccualtion model captures some general phenomena known from experiments, in particular the prediction of a minimum in flocculation intensity after the step of a sudden pipe expansion, and the subsequent re-flocculation process. Varying the fibre properties, i.e. fibre length and diameter, different behaviors of the flocculation intensity evolution in a planar contraction is predicted for typical headbox flows. Longer fibres are activated easier and from an equilibrium state at the inlet the flocculation intensity increases throughout the contraction. A shorter fibre such as birch will predict the opposite. In addition both long and short fibres will give an increase in flocculation intensity starting from a non-equilibrium state at low intensity. This trend is supported by experimental results from the literature.

An Eulerian propability density function is determined by solving a convection-dispersion equation describing the evolution of fibre orientation in a combined extensional and shear flow. This numerical approach is used to evaluate the effect of turbulence generating vanes and wall boundary layers on fibre orientation distribution in a planar contraction. The boundary layer will for both in the plane of paper and in the plane of contraction wider the fibre orientation distributions, i.e the fibres will be less oriented. For the outlet profile of the contraction the fibre orientation distribution will be more effected by the blunt vane tip than the tapered vane tip. The model is validated with experimental results in literature and a good qualitative agreement was achieved.

Descriptors: fibre suspension, fibre flocculation, fibre orientation, flow contraction, pipe expansion, headbox, turbulent flow, anisotropy

List of papers

Appended papers:

Paper 1. Hyensjö, M., Hämäläinen, J. P., and Dahlkild, A., 2003 Turbulent dilute fibre suspension flow modelling in a circular pipe enlargement. In, Proceedings of the 89^{th} Annual PAPTAC Meeting, Montreal, Canada

Paper 2. Hyensjö, M., Dahlkild, A., A numerical study on mechanical fibre flocculation in a planar contraction. To be submitted

Paper 3. Hyensjö, M., Krochak, P., Olson, J., Hämäläinen, J. and Dahlkild, A., 2004 Modelling a turbulent dilute fibre suspension in a planar contraction: Effect of vane types, vane position and wall boundary layer on fibre orientation distribution. In *Proceedings of the 5^{th} International Conference on Multiphase Flow, ICMF'04*, Yokohama, Japan

Division of work between authors

Paper 1: Marko Hyensjö (MH) implemented the model into the CFD code. All numerical modelling was carried out by MH. The manuscript was prepared by MH under the supervision of Jari Hämäläinen (JH) and Anders Dahlkild (AD).

Paper 2: Modelling and implementation was carried out by MH under the guidance of AD. The manuscript was prepared by MH with support, discussion and guidance of AD.

Paper 3: Numerical algorithms and implementation were developed by MH and Paul Krochak (PK). The ideas behind the paper are contribution from all the authors. MH prepared the manuscript and with comments and discussion with the other authors.

Contents

CHAPTER 1

Introduction

One of the key component of a papermachine is the forming section. This is, as the name reveals, where the paper is formed from a cellulose fibre suspension into a paper web. Within the forming section two main components are included, namely the headbox and the former. Besides the forming criteria of the headbox, it also has the capability to distribute the fibre suspension evenly into a jet, e.g. 10m wide and 10mm thick, for speeds up to 2200 m/min. Furthermore is the cross directional basis weight and fibre orientation controlled by means of dilution control and slice lip micro adjustment respectively. In a headbox sheets/vanes/wedges are used for different purposes. It can be used e.g. for better formation, lower the ratio between the strength in the machine direction (MD) and the strength in the cross direction (CD) or as separating layers for multi-layering capability. For Tissue paper grades multi-layering or

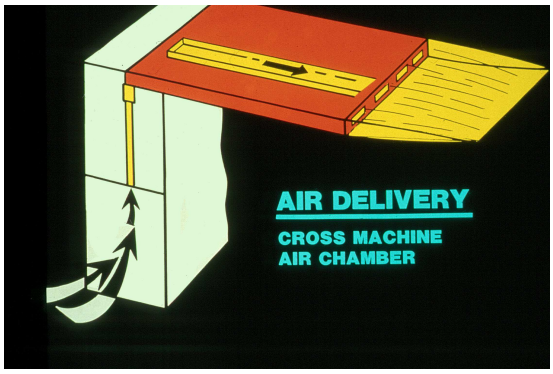

FIGURE 1.1. KMW air-wedge technology with purge of excess air between jets, Andersson (1982)

stratified forming is a key feature of the headbox. The application of this technology started in mid 70's. Within former Beliot Corporation the Strataflo headbox was introduced in which flexible sheets were used to separate the layers. At KMW Development Center in Karlstad, Gunnar Stenberg introduced the air-wedge technology separating the layers thus reducing the mixture of the layers. Into this air wedge also excess air was purged to control the reattachment point between the jets and as a stabilization of the jets, cf. Figure 1.1.

The basic principle was to decrease the velocity gradients within the separated jets before they attach and to keep the individual jets separated all the way into the drainage zone, cf. Stenberg (1979), Andersson (1982) and Andersson (1984). The historical development of the multi-layer Tissue headbox within Metso Paper was starting with the HTB type with air-wedge and lately with vanes. Thereafter the SymFlo TIS headbox was introduced in the beginning of the 90's. The latest Tissue multi layer headbox is the OptiFlo II TIS with wedges that separates the layers, cf. Figure 1.2. New hydraulics in combination with wedges will reduce the flocculation process and therefore improve formation in this headbox, with maintained layer purity.

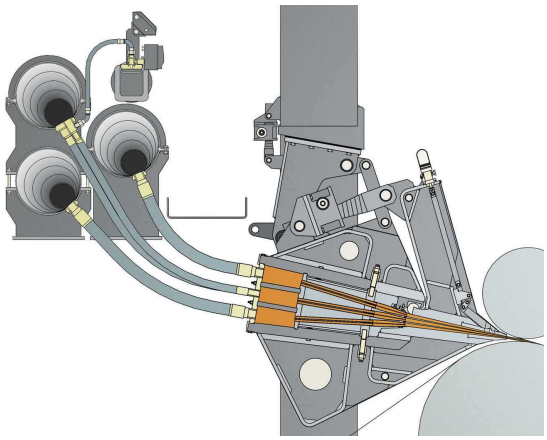

FIGURE 1.2. The latest multi layer headbox within Metso Paper is the OptiFlo II TIS with wedges

1.0.1. *Outline of thesis*

The first part of the thesis presents a summary section of the papers covered and the second part consists of the papers. Two main modelling areas have been considered in this thesis, i.e. mechanical fibre flocculation and fibre orientation. For a numerical modelling of a cellulose fibre suspension in water, difficulties will arise with a multi-phase description due to the flexible long fibres and their many interactions with each other. In modern headboxes the flow is of turbulent nature, therefore this will be the key feature of the modelling approach. Examples of studies reported in the literature to model fibre suspensions in turbulent flows are, e.g. Andersson (1966) , Hourani (1988*a*), Hourani (1988*b*), Steen (1990), Steen (1993), Plikas *et al.* (2000), Kuhn & Sullivan (2001) and Hyensjö *et al.* (2003). The aim is to develop useful tools for the industry when studying the effect of headbox geometry, flow rate and fibre type on fibre orientation, flocculation and formation.

CHAPTER 2

Mechanical fibre flocculation modelling

Cellulose fibres dispersed in water tend to form aggregates, i.e. flocs, due to mechanical and nonmechanical factors, studied experimentally by e.g. Mason (1954), Norman *et al.* (1977) and Kerekes (1983). The state of these aggregates in the forming section of a papermachine, i.e. the headbox and the former, determines the formation of the final paper made. For a numerical modelling of a cellulose fibre suspension in water, difficulties will arise with a multi-phase description due to the flexible long fibres and their many interactions with each other. A typical number of particles, at a papermaking consistency of 1%, for one cubic centimeter can be up to $3.0 \cdot 10^4$ particles. For the complex geometries typically found in paper machine equipment this will exclude any lagrangian approach, i.e. based on solving the equations of motion for an individual particle in a given flow field. Examples of studies that are reported in the literature to model fibre suspensions in turbulent flows are, e.g. Andersson (1966) , Hourani (1988*a*), Hourani (1988*b*), Steen (1990), Steen (1993), Plikas *et al.* (2000), Kuhn & Sullivan (2001) and Hyensjö *et al.* (2003). The model proposed by Steen, i.e. the Fibre Flocculation Concept (FFC), is based on a one-phase description of the fluid flow. In his model the fibrous phase is only described by the flocculation intensity solved as a passive scalar variable. The result of this approach is that the effects of the fibre phase on a main flow (i.e. average water flow and turbulence) are neglected. The FFC is based on the governing equation for a general scalar fluctuation, e.g. Rodi (1993). The rupture term, i.e. the dissipation term, is similar to the one derived by Rodi (1993) but the aggregation term, i.e. the production term is different. The production of a scalar fluctuation is usually controlled by mean scalar gradients, while the flocculation aggregation in the FFC is based on that floc aggregation starts out as a small scale activation of fibres followed by floc collisions and fibre network settling, cf. Steen (1990) and Steen (1993). In the work by Plikas *et al.* (2000) and Kuhn & Sullivan (2001), a similar analogy with a general scalar fluctuation is used. However both dissipation and production terms are based on model constants which are calibrated against experimental data by Moayed (1999). This makes it applicable only for that particular grid-generated turbulence flow cell.

The FFC by Steen is investigated in a planar contraction and a sudden pipe expansion, which is a typical geometry in a headbox. Two slightly different versions of FFC is reported named here as FFC-1990 and FFC-1993, cf. Steen

(1990) and Steen (1993). The FFC-1990 is studied with the sudden pipe expansion, while for the planar contraction both versions of the FFC are applied and the result of the different versions are presented and the difference of them are discussed. The effect of various parameters, e.g. fibre properties, i.e. fibre length and diameter, flow rate and the state of the fibre suspension on aggregation are studied. Finally observe that this study considers only the dilute consistency regime, i.e. <1%, which is expected in papermaking.

2.1. Sudden Pipe Expansion

The position of the maximum turbulent kinetic energy downstream of a circular-to-circular pipe expansion, has its approximate location slightly upstream of the re-attachment point for a pure fluid. In the experimental work by Karema *et al.* (2001), they showed that the maximum of the turbulent fluctuations of the fibrous phase and the minimum floc volume also coincide approximately with this location. Their measurement of the turbulent state of the fibrous phase was done with a pulsed ultrasound-Doppler anemometer. Also d'Incau (1989) clearly showed experimentally that the maximum strain rate and minimum macro length scale coincide at approximately the same position. The assuming cylindrical symmetry of flocs gives the definition of the dimensionless floc volume to be the projected length component in the streamwise direction times the projected length component in transverse direction squared divided by the cubic of the average fibre length, cf. Karema *et al.* (2001). The measured dimensionless floc volume for PPP3 geometry and for Pine at 0.5% consistency for different flow rates shows a decreasing minimum floc volume with increasing flow rate, cf. Figure 2.1, Karema *et al.* (2001). The same trend was found by Moayed (1999), measuring the flocculation intensity. The result of Karema et al. in Figure 2.1, also show how the curves seem to almost collapse into a common line independent of the flow rates from the point of minimum floc size and forward. CFD simulations were performed for the same geometry and flow rates as used by Karema et al. shown in Figure 2.1. The flocculation intensity values for the respective axial position were calculated as area weighted averages of the flocculation intensity field, cf. Figure 2.2 and the definition of flocculation intensity in equation (2) in Paper 1 and 2. Also here the curves seem to collapse into a common curve. The minimum values are not that pronounced as in Figure 2.1, but the general trend is the same, i.e. increasing flow rate decreases the minimum value and vice versa. Furthermore the values tend to reach a saturation level for the respective flow rate. This type of saturation behaviour can be seen for another geometry with a smaller step and the same pulp, cf. Karema *et al.* (2001). I the case of birch pulp, i.e. shorter fibres, these authors found that the pronounced minimum after the step for the same geometry and flow rate, was absent. Further the figures clearly show that the time scales differs since in the experimental data the flocs seem to grow at a slower rate than for the simulations. This still shows that even with the "non-tuned" FFC the simulations catch some of the physical behaviour. The diffusivity of the flocculation intensity was varied, to be able to study the

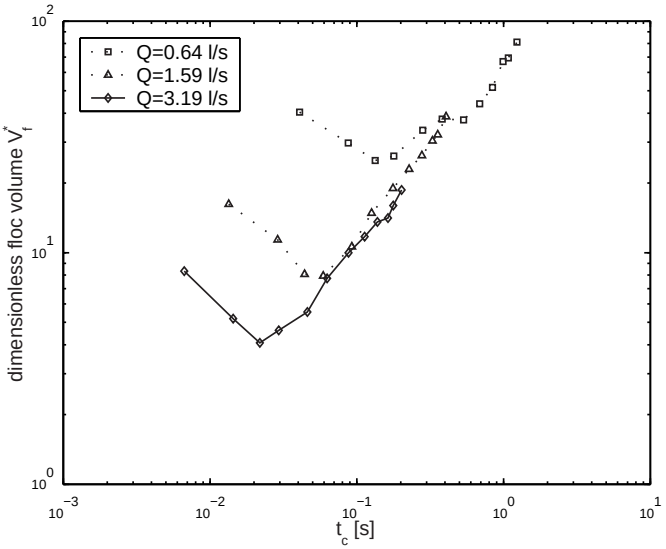

FIGURE 2.1. Dimensionless floc volume vs. mean residence time from the step, cf. Karema et al. (2001)

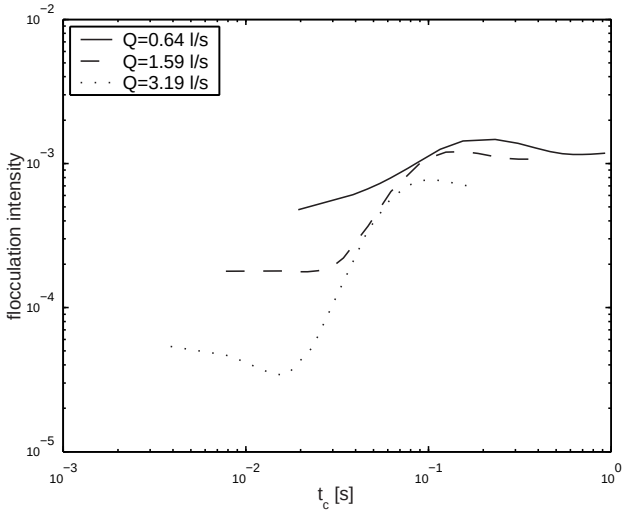

FIGURE 2.2. CFD simulated flocculation intensity as a function of mean residence time from the expansion

influence on the flocculation intensity profile, cf. Figure 2.3. The simulations were carried out for a flow rate of 1.59 l/s in a straight pipe with the inner diameter of 26 mm. In the paper by Steen (1990), the effective diffusivity was

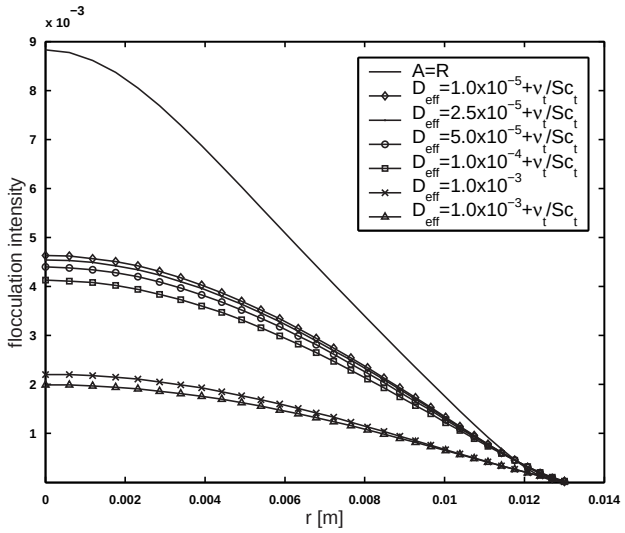

FIGURE 2.3. Effect with various effective diffusivities on the flocculation intensity profiles for a fully developed pipe flow

arbitrary set equal to 0.001. This includes both the kinematic and turbulent diffusivity when introduced in the equation for a passive non-reacting scalar variable in our case cf. equation (1) in Paper 1. For a fully developed fluid flow in a pipe the convective term vanishes. Therefore for vanishing effective diffusivity only the source term would be significant, and by setting this term equal to zero, i.e. $A = R$, it is possible to solve for a fully developed flocculation intensity profile in the case $D_{eff} = 0$, cf. Figure 2.3. The figure clearly shows how the presence of diffusivity to various degrees evens out the flocculation intensity profile. The various effective diffusivity models used are indicated in the legend of Figure 2.3. When decreasing the kinematic diffusivity the centre value, i.e. the peak value, goes asymptotically to a given value. This means that the diffusivity is dominated by turbulent diffusivity, cf. Figure 2.3 case $D_{eff} = 1.0 \cdot 10^{-5} + \nu_t/Sc_t$.

2.2. Planar Contraction

The evolution of flocculation along the centerline in a planar contraction is here quantified with the normalized flocculation intensity, ϕ/ϕ_0 ($\phi_0 = 3.57 \cdot 10^{-3}$), cf. Figure 2.4. The inlet flocculation intensity value, ϕ_0, was obtained from the aggregation term, A, set equal to the rupture term, R, with given k_0 and ε_0, which corresponds to a fully developed flocculation field with a vanishing convective term, and with the effective diffusivity term neglected. Two different turbulence models with FFC-1990 are compared, the k-ε and the Reynolds Stress model (LLR-IP). Also for the Reynolds Stress model two different boundary conditions for the flocculation intensity, ϕ, are tested, zero value, $\phi = 0$,

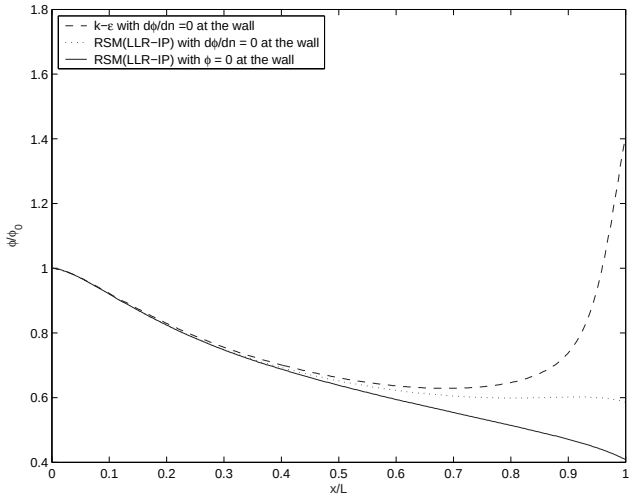

FIGURE 2.4. Normalized flocculation intensity with inlet value along centerline of the contraction for different turbulence models with FFC-1990

and zero gradient at the wall. As can be seen the k-ε turbulence model will give a non physical behavior of the flocculation intensity development due to factors described in Paper 2. The Reynolds Stress Model (LLR-IP) gives a more accurate description of the turbulence and therefore a more realistic description of the flocculation behavior in a planar contraction. The outlet value of the flocculation intensity is dependent on which boundary condition for ϕ that is chosen. The case with isolated wall boundary condition, dϕ/dn=0, gives the highest flocculation intensity outlet level. This due to the fact that the quantity, ϕ, is globally preserved in the planar contraction. The result from the two versions, FFC-1990 and FFC-1993, are shown in Figure 2.5. These simulations are made with the RSM (LLR-IP) turbulence model and with dϕ/dn=0 at the wall and an even mean consistency is assumed for both FFC-1990 and FFC-1993. The difference in result for the equilibrium inlet of the flocculation intensity between the versions are striking. The flocculation intensity at the inlet $\phi_0 = 2.39 \cdot 10^{-9}$ for FFC-1993 which is six orders of magnitude lower that for the FFC-1990. Now increasing the velocity to typical headbox flows, i.e. 10 times the flow in Figure 2.4 and 2.5. This will furthermore reduce the time scale, which is important for the flocculation process, cf. Karema *et al.* (2001). The importance of time when increasing the velocity, thus reducing the time scale, is predicted with FFC-1990, cf. Figure 2.6. The inlet turbulence level, i.e. k_o and ε_0, is kept the same for the different velocities, and this corresponds turbulence intensities 5.45%, 4% and 2.73% with increasing velocity respectively. As can be seen in Figure 2.6 a), a jet velocity of 33.33 m/s, have

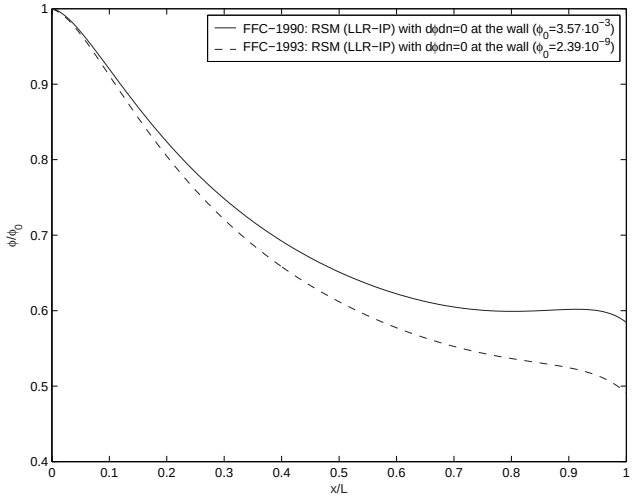

FIGURE 2.5. Normalized flocculation intensity with inlet value along centerline of the contraction for the two different versions FFC-1990 and FFC-1993

the shortest residence time in the contraction and therefore the lowest outlet flocculation intensity value. In Figure 2.6 b), the normalized flocculation intensity with normalized position along the contraction is shown. The convective dependency or the time scale is also here illustrated giving a lower normalized flocculation intensity gradient with increasing velocity. Note that for velocities typical of headbox flows the flocculation intensity value will increase from an equilibrium inlet value in contrast with the case earlier, cf. Figure 2.6, 2.4 and 2.5. Experimental result by VTT Energy/Metso Paper Inc. provides some results on the development of floc length in CD direction for different outlet jet velocities in a planar contraction for a Birch fibre, cf. Figure 2.7. As can be seen the floc size for the particular contraction will increase, i.e. reflocculation takes place in the contraction. This was also demonstrated by Karema *et al.* (2001) in a contraction with vanes. In Figure 2.8 a) the modelled flocculation intensity evolution with FFC-1990 for a planar contraction with fibre dimensions, l=3mm and d= $30\mu m$ is shown and in b) with fibre dimension for Birch, i.e. l=0.96mm and d= $18.9\mu m$. The modelled result shows different behavior for the case starting from an equilibrium state. The Birch fibre will decrease through out the contraction while the longer fibre will increase in flocculation intensity. The experimental result in Figure 2.7 indicates that the floc volume will increase for a planar contraction. For the non-equilibrium case, $0.01\phi_0$, both fibre dimension cases predict an increase in flocculation intensity.

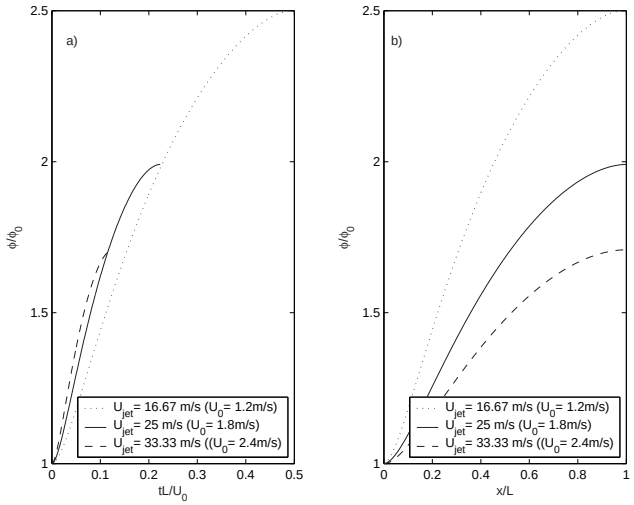

FIGURE 2.6. a)Development of the normalized flocculation intensity with increasing flow rate for FFC-1990 with residence time. b) The normalized flocculation intensity with normalized position along the contraction

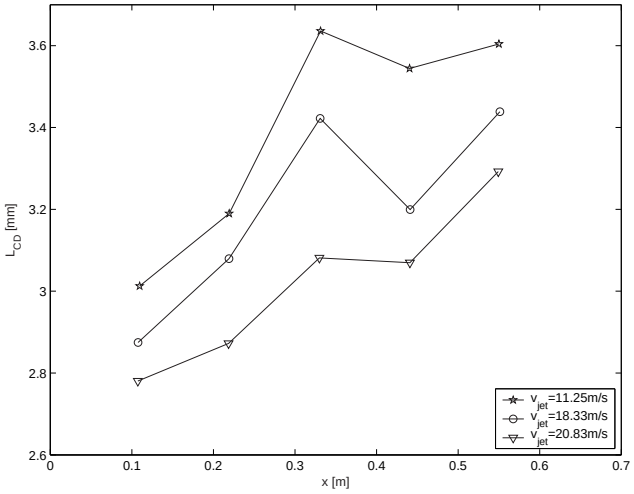

FIGURE 2.7. Experimental result of CD floc length in a planar contraction by permission from Metso Paper Inc/VTT Energy Jyväskylä, Finland. Birch fibre dimensions: l=0.96mm and d= 18.9μm.

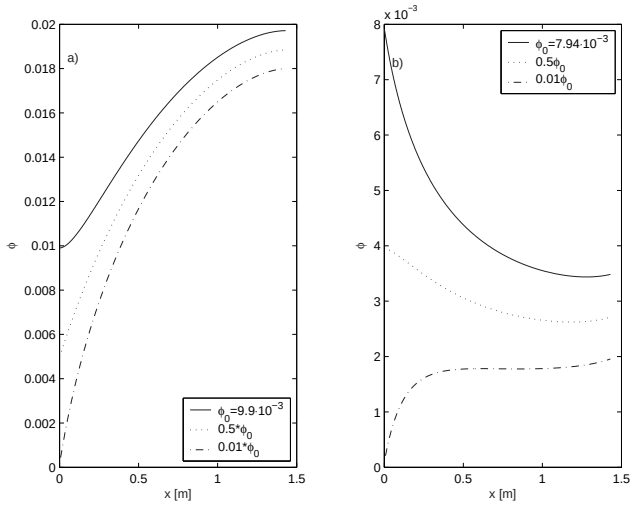

FIGURE 2.8. a) Modelled flocculation intensity with FFC-1990 in planar contraction with fibre dimensions: l=3mm and d= $30\mu m$. b) Modelled flocculation intensity with FFC-1990 in planar contraction with Birch fibre dimensions: l=0.96mm and d= $18.9\mu m$.

CHAPTER 3

Fibre orientation distribution modelling

The paper strength properties in machine direction and cross-machine direction as well as in thickness direction (i.e. z-direction) are important for the runnability and dimensional stability of the paper sheet in copying and printing machines. The strength properties are determined by chemicals, fibre type and preparation, but also largely by anisotropy of fibre orientation distribution. Many of the final paper properties is based upon the state of the fibre suspension in the early stage of the process, e.g. Norman & Söderberg (2001). As the jet hits the moving fabric the state or the history of this jet is essential. The jet is formed in the so called headbox. The headbox ensures that the jet leaves with a specific state depending on the type of paper web to be produced. The interaction between this jet and the moving fabric(s) is a main feature for achieving the desired final result. For example in high speed printing it is desirable to have high tensile strength in the direction of the paper feed. For other application such as sack paper it is required to have a uniform distribution and orientation distribution of the fibres. The state of the jet can be modified in various ways. One way is to vary the contraction ratio, i.e. the ratio between the inlet height and outlet height of the contracting channel. By increasing the contraction ratio it is known that it significantly increases the fibre alignment, e.g. Ullmar (1997), Ullmar (1998) and Zhang (1998), and this can essentially change the final paper properties, e.g. Nordström & Norman (1994) and Söderberg & Kiviranta (2003). Other ways is to insert vanes into the contracting channel of the headbox. These vanes, depending on their shapes and lengths, generate turbulence and this can disperse and disorient fibres, i.e result in a more uniform sheet by means of final strength of the paper. The effect of the vane tip location on fibre mixing was experimentally studied by Lloyd & Norman (1998). This was done by dying a layer of pulp fibres blue, passing them through a hydraulic headbox and then scanning a finished sheet of paper for the variation of blue content. Their results showed that different vane locations can in fact lead to different levels of mixing. Conventional headboxes use also a slice bar near the exit to control the cross machine direction (CD) basis weight profile. Simultaneously it also affects the fibre orientation angle. When modern headboxes of today utilizes dilution water to control the CD basis weight profile, the slice bar can be used to adjust the fibre orientation angle profile. Unfortunately very little is known on neither the effect of turbulence vanes, nor on the effect of a slice bar or headbox geometries, all of

which can have a significant effect on fibre orientation anisotropy.
The main purpose of this study is to use numerical modelling to evaluate the effect of turbulence generating vanes and wall boundary on fibre orientation distribution in a planar contraction. An approach to use the CFD modelling as an input for the extended one dimensional headbox model is illustrated. Earlier modelling studies have neglected the influence of turbulence in an accelerated fluid flow, e.g. Zhang (1998), Olson (2002) and Akbar & Altan (1992). The rotational dispersion coefficient, in the extended one dimensional headbox model, will be determined by correlating the CFD analysis with experimental data presented in the work by Ullmar (1998). The rotational dispersion coefficient has been related to turbulence quantities, cf. Olson & Kerekes (1998), Olson (2001) and Krushkal & Gallily (1988). The relationship is based on Kolmogoroffs local isotropic hypothesis for very small eddies of the turbulence spectrum, cf. Equation (4) in paper 3. In the experimental work by Asplund & Norman (2003), the fibre orientation anisotropy in a jet after a planar contraction with vanes was studied. Result from this study has been used as a validation and comparison of the extended one dimensional headbox model.

3.1. Fibre Orientation Distribution

The convection-dispersion equation describing the evolution of fibre orientation in a one dimensional headbox, as derived by Olson *et al.* (2004), is here extended to be valid for an arbitrary streamline. The extended one dimensional headbox model is then given for a coordinate system, s, following a streamline as:

$$\frac{\partial \Psi}{\partial t} + U_s \frac{\partial \Psi}{\partial s} = D_p \frac{\partial^2 \Psi}{\partial \phi^2} - \frac{\partial (\dot{\phi} \Psi)}{\partial \phi} \tag{3.1}$$

where s is defined as the square root of the sum of the squared values of the plane coordinate variables, x and y resp., and U_s is the tangential average velocity along the streamline. Note that even though we are following a streamline this is still a Eulerian approach since we are not following individual fibres. D_p is the rotational dispersion coefficient and ϕ is the projected angle in the plane of contraction. The first term is the time derivative of the fibre orientation distribution. Equation (3.1) is simplified by assuming steady flow, and made dimensionless with the scaled variables $\overline{s} = \frac{s}{L_s}$ and $\overline{U_s} = \frac{U_s}{U_0}$, where L_s is the length of the streamline considered. This gives the following expression for fibre orientation in the plane of contraction along a streamline:

$$\overline{U_s} \frac{\partial \Psi}{\partial \overline{s}} = \overline{D_p} \frac{\partial^2 \Psi}{\partial \phi^2} - \frac{\partial}{\partial \phi} (\dot{\phi} \Psi) \tag{3.2}$$

In previous work, a convection-dispersion model of fibre orientation in a one dimensional headbox was derived and numerically studied by Olson *et al.* (2004). The model accounts for a constant value, 2.5, of the dimensionless rotational dispersion coefficient and it was shown to agree well with the independent findings of Ullmar (1998). The constant in the dimensionless rotational dispersion coefficient presented in equation (3.3) has been determined and validated with

the results presented by Ullmar (1998). This resulted in the following correlation:

$$\overline{D_p} = 6.57 \times 10^{-2} \frac{L_s}{U_0} (\frac{\varepsilon}{\upsilon})^{\frac{1}{2}} \tag{3.3}$$

This result is about 5.5 times smaller than the proposed value by Olson (2001). In the work by Olson (2001) this expression was derived for isotropic homogeneous turbulence, which is not the case here.

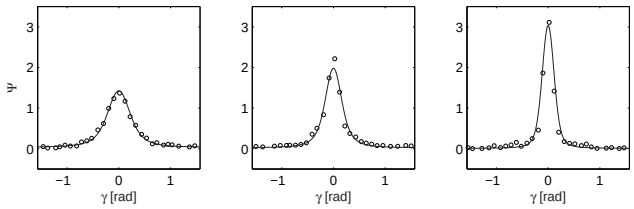

FIGURE 3.1. Predicted and measured, Ullmar (1998), fibre orientation distributions for contraction ratios of 16.7, 25, 50.

In Figure 3.1 results for different contraction ratios of 16.7, 25 and 50, of the proposed correlation in equation (3.3) compared to experimental data of Ullmar (1998) can be seen. These results are from the outlet in the centerline of the contraction and made in the plane of paper, i.e. γ. This suggest a good agreement between the predicted and measured data for the different contraction ratios. This also demonstrates the enhanced alignment of fibres for an increased contraction ratio. The dimensionless rotational turbulent dispersion in Equation (3.3) is used for both γ and ϕ.

3.2. Results

Since the fibre orientation distributions for γ are nearly Gaussian distributions the degree of fibres not being oriented towards γ=0 is represented by the standard deviation $\sigma(\gamma)$:

$$\sigma_\gamma^2(x,y) = \int_{-\frac{\pi}{2}}^{+\frac{\pi}{2}} \gamma^2 \Psi(\gamma,x,y) d\gamma \tag{3.4}$$

$\Psi(\gamma,x,y)$ is here the normalized distribution function for γ on the interval $-\pi/2 \leq \gamma \leq +\pi/2$. For ϕ we may make an analogous definition:

$$\sigma_\phi^2(x,y) = \int_{-\frac{\pi}{2}}^{+\frac{\pi}{2}} (\phi - \phi_m)^2 \Psi(\phi,x,y) d\phi \tag{3.5}$$

where $\Psi(\phi,x,y)$ is the distribution function for ϕ. One may observe that, although the mean value of ϕ taken over a complete cross section of the channel is zero, this is not necessary the case for the local mean value $\phi_m(x,y)$, cf. Figure 3.2. Figure 3.2 shows the local mean value, ϕ_m, across the outlet section,

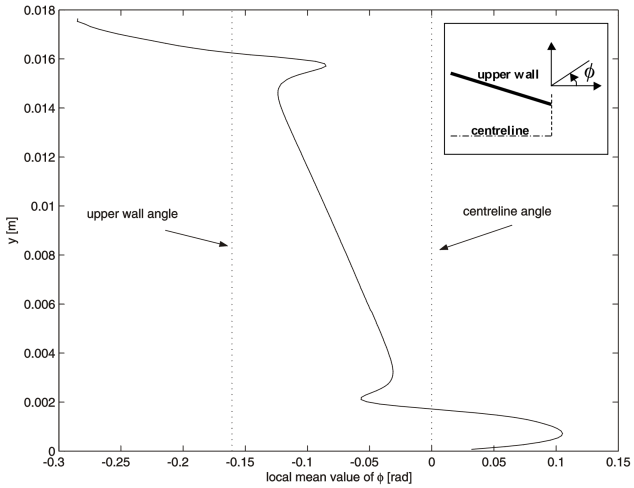

FIGURE 3.2. Outlet profile of the local mean value of ϕ for a tapered vane at vane position -80 mm from the outlet.

from the centreline and to the upper wall. The overall trend at the outlet is a mean orientation basically along the local flow direction, gradually approaching the inclination of the upper wall for increasing distance from the centreline. Deviations from this trend appear in the shear layers of the wake and the wall, where fibres close to the wall have a mean angle less than the upper wall it self and fibres in the lower part of the wake have a positive mean angle. The effect of vane position is presented in Figure 3.3. The closer the vane is to the outlet the larger is the effect on the σ_ϕ. This trend is similar to experimental data for the fibre orientation anisotropy, cf. Asplund & Norman (2003). In their work for a thick, blunt vane tip at a mean velocity of 5 m/s, the undisturbed region was vanishing as the vane tip was moved closer to the outlet.

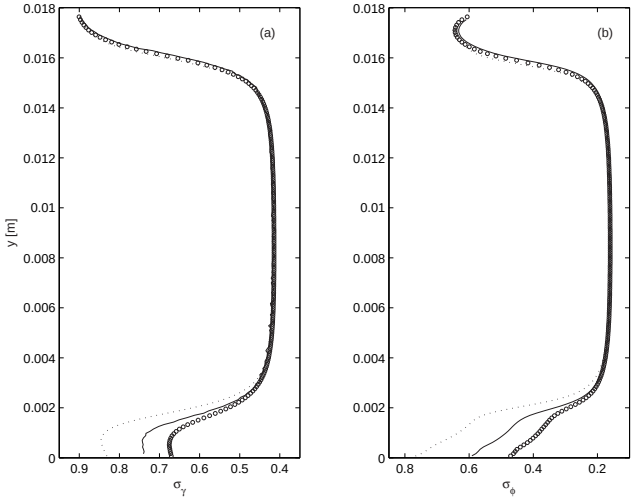

FIGURE 3.3. Standard deviation outlet profiles for γ (a) and ϕ (b), at different vane positions: -80 (..), -230 (-) and -380 (o) mm from the outlet, for a tapered vane tip.

CHAPTER 4

Concluding remarks

The fibre floccualtion model captures some general phenomena known from experiments, in particular the prediction of a minimum in flocculation intensity after the step of a sudden pipe expansion, and the subsequent re-flocculation process. Varying the fibre properties, i.e. fibre length and diameter, different behaviors of the flocculation intensity evolution in a planar contraction is predicted for typical headbox flows. Longer fibres are activated easier and from an equilibrium state at the inlet the flocculation intensity increases throughout the contraction. A shorter fibre such as birch will predict the opposite. In addition both long and short fibres will give an increase in flocculation intensity starting from a non-equilibrium state at low intensity. This trend is supported in experimental result from the literature.

The use of this one-phase approach with the FFC shows on a need of a modification of the turbulence model, which takes into account additional production and dissipation. There is a lack in literature of such modifications in turbulence for the presence of flexible long fibres or aggregates of fibres, i.e. flocs.

An Eulerian propability density function is determined by solving a convection-dispersion equation describing the evolution of fibre orientation in a combined extensional and shear flow. This numerical approach is used to evaluate the effect of turbulence generating vanes and wall boundary layers on fibre orientation distribution in a planar contraction. The boundary layer will for both in the plane of paper and in the plane of contraction wider the fibre orientation distributions, i.e the fibres will be less oriented. For the outlet profile of the contraction the fibre orientation distribution will be more effected by the blunt vane tip than the tapered vane tip. The model is validated with experimental results in literature and a good qualitative agreement was achieved.

Shear flow is used today to break flocs in the turbulence generator of the headbox. It is shown that turbulence is good at dispersing flocs as in other applications, but the decay of turbulence is also effective in reflocculating the fibres into aggregates once again. One solution is to use extensional flow to break flocs which has be shown in literature to be more efficient, or combination of such flows. From a numerical modelling point of view, a combination of a flocculation model with a floc/fibre orientation would be of interest. The essential validation of such numerical models needs experiments.

Acknowledgements

I would like to thank Metso Paper Inc./Metso Academy and the Swedish Research Council for the financial support of the project. Moreover I would like to thank my supervisor at KTH, Docent Anders Dahlkild for being patient, helpful and supporting during long and fruitful discussions. I would also like to thank Professor Jari Hämäläinen being my former supervisor and the present supervisor Tekn.Dr. Tomas Wikström within Metso Paper Inc. Furthermore I would like to thank colleagues, Paul Krochak, James Olson, Mark Martinez and others, at the Pulp and Paper Center at UBC, giving me new experiences during my stay in Vancouver in the summer of 2003. Also people at the paper technology group within FaxénLaboratoriet is acknowledged. Within Metso Paper Karlstad I would like to acknowledge Carl Zotterman, Ingvar Klerelid and Torbjörn Wahlström for discussions and giving me the opportunity working with the project. Last but not least I would deeply like to thank my Family, Annie, Henrik and Carl.

Bibliography

Akbar, S. & Altan, C. 1992 On the solution of the fibre orientation in two-dimensional homogeneous flows. *Polymer Eng. Sci.* .

Andersson, I. 1982 Simultaneous forming of multi-layer products with the kmw air wedge technology. In *In Proceeding of Papex '82 International - "Papermaking in the Eighties"* (ed. Y. PITA, Harrowgate), pp. 86–97.

Andersson, I. 1984 Multi-layering on a roll former. In *In Proceeding of SPCI The World Pulp and Paper Week - New Available Techniques"*, pp. 157–163.

Andersson, O. 1966 Some observation on fibre suspensions in turbulent motion. *Svensk Papperstidning* **69(2)**, 23–31.

Asplund, G. & Norman, B. 2003 Fibre orientation anisotropy profile over the thickness of a headbox jet. *89th Annual PAPTAC Meeting, Montreal* .

d'Incau, S. 1989 Characteristic of the decay of turbulence in a pulp suspension flow. *International Journal of Multiphase Flow* **15(5)**, 735–746.

Hourani, M. 1988*a* Fiber flocculation in pulp suspension flow part1: Theoretical model. *Tappi Journal* pp. 115–118.

Hourani, M. 1988*b* Fiber flocculation in pulp suspension flow part2: Experimental results. *Tappi Journal* pp. 186–189.

Hyensjö, M., Hämäläinen, J. P. & Dahlkild, A. 2003 Turbulent dilute fibre suspension flow modelling in a circular pipe enlargement. *89th Annual PAPTAC Meeting, Montreal* .

Karema, H., Salmela, J., Tukiainen, M. & Lepomäki, H. 2001 Prediction of paper formation by fluidisation and reflocculation experiments. *12th Fundamental Research Symposium* pp. 559–589.

Kerekes, R. 1983 Flocculation in decaying turbulence: A literature review. *J. Pulp Paper Sci.* pp. TR86–TR91.

Krushkal, E. M. & Gallily, I. 1988 On the orientation distribution function of non-sperical aerosol particles in a general shear flow - ii. the turbulent case. *Journal of Aerosol Science* **19**, 197–211.

Kuhn, D. & Sullivan, P. 2001 Analysis and measurement of the flocculation intensity of a flowing pulp suspensions. *"2001 Papermakers Confenrence, Cincinatti, OH, USA* .

Lloyd, M. D. & Norman, B. 1998 Layer mixing during three-layer stratified formning: The role of vane lenght and mix-wire speed difference. *Tappi Journal* pp. 194–201.

Mason, S. G. 1954 Fibre motions and flocculation. *Pulp and Paper Magazine of Canada* **55** (13), 96–102.

Moayed, R. 1999 Characterization of fibre suspension flows at papermaking consistencies. PhD thesis, Department of Chemical Engineering and Applied Chemistry, University of Toronto, 1999, Toronto, Canada.

Nordström, B. & Norman, B. 1994 Influence on sheet anisotropy, formation, z-toughness and tensile stiffness of reduced feed area to a headbox nozzle. *Nordic Pulp and Paper Research Journal* **1(9)**, 53–59.

Norman, B., Möller, K., Ek, R. & Duffy, G. 1977 Hydrodynamics of papermaking fibres in water suspension. In *Fibre - Water Interactions in Papermaking: Transactions of the Symposium held at Oxford: September 1977*, , vol. 1(2), pp. 195–249.

Norman, B. & Söderberg, D. 2001 Overview of forming literature, 1990-2000. *Trans. 12th Fundamental Research Symposium, Oxford* **1**, 431–558.

Olson, J. A. 2001 The motion of fibres in turbulent flow, stochastic simulation of isotropic homogeneous turbulence. *International Journal of Multiphase Flow* **27**, 2083–2103.

Olson, J. A. 2002 Analytical estimate of the fibre orientation distribution in a headbox flow. *Nordic Pulp and Paper Research Journal* **3 (17)**, 302–306.

Olson, J. A., Frigaard, I., Chan, C. & Hämäläinen, J. P. 2004 Modelling a turbulent fibre suspension flowing in a planar contraction: The one-dimensional headbox. *International Journal of Multiphase Flow* **30**, 51–66.

Olson, J. A. & Kerekes, R. J. 1998 The motion of fibres in turbulent flow. *Journal of Fluid Mechanics* **377**, 47–64.

Plikas, A., Kuhn, D. & Sullivan, P. 2000 A numerical model of fibre suspensions in a grid generated turbulent flow. In *ASME 2000 Fluids Engineering Division Summer Meeting: Proceedings of ASME FEDSM'00 held in Boston, Massachusetts, USA*, pp. 991–996.

Rodi, W. 1993 *Turbulence Models and Their Application in Hydraulics A State-of-the-art review*, 3rd edn. IAHR-AIRH, A.A.Balkema, Rotterdam.

Söderberg, D. & Kiviranta, A. 2003 Improvement of base-ply formation through headbox modification. *89th Annual PAPTAC Meeting, Montreal* .

Steen, M. 1990 Modelling fibre flocculation in turbulent flow; a numerical study. *TAPPI Engineering Conference, Seattle, USA* pp. 475–486.

Steen, M. 1993 On turbulence and flocculation in fibre suspensions. *Institue of Paper Science and Technology, Atlanta, Georgia USA* .

Stenberg, G. 1979 Patent specification, kmw. *SE 7804729-7* .

Ullmar, M. 1997 Observations of fibre orientation in a headbox model at low consistency. *Tappi proceedings, Engineering and Papermakers Conference* p. 865.

Ullmar, M. 1998 On fibre alignment mechanisms in a headbox nozzle. *Licentiate Thesis, Royal Institute of Technology, Stockholm, Sweden* .

Zhang, X. 1998 Fibre orientation in a headbox. *Masters Thesis, The University of British Columbia, Vancouver, Canada* .

Paper 1

1

Turbulent Dilute Fibre Suspension Flow Modelling in a Sudden Circular Pipe Enlargement

By Marko Hyensjö[1,2], Jari P Hämäläinen[2] and Anders Dahlkild[3]

[1]Metso Paper Karlstad AB, P.O. Box 1014, SE-651 15 Karlstad, Sweden
[2]Metso Paper Oy, P.O. Box 587, FIN-40101 Jyvskylä, Finland
[3]FaxnLaboratoriet, KTH, SE-100 44 Stockholm, Sweden

In proceedings of the 89^{th} Annual PAPTAC Meeting, Montreal, Canada

This paper introduces a comparison between CFD simulations and experimental data of a dilute fibre suspension flow in an expanding step. In this model the fibrous phase is described only by the flocculation intensity solved as a passive scalar variable. Even when using the "non-tuned" Fibre Flocculation Concept (FFC) it captures some general behaviour that is expected, thus prediction of a minimum after the step and the re-flocculation process. The curves for the re-flocculation process seem to collapse into a common curve, which is consistent with experimental data. The study also shows that in CFD simulations for increasing flow rate the minimum value of the measure of flocculation decreases at the same rate as experimental data, with an underestimation for the higher flow rates. Furthermore CFD simulations and experimental data showed that the time scales differ. In the experimental data the flocs seem to grow at a slower rate than for the simulations. However, the qualitative picture of the flocculation process is definitely captured by the FFC. Thus the model is a useful tool in R&D when studying the effect of headbox geometry and flow rate on flocculation and formation.

---

1. Introduction

One of the most focused properties of a paper sheet is the formation. A good dispersion of fibres, equivalent to a good formation, is necessary to insure good mechanical properties of the paper, e.g. Andersson & Steen (1962) and Norman & Söderberg (2001). The formation is defined as the small-scale basis weight variations up to about 40 mm in wavelength, cf. Norman & Wahren (1972) and Norman (1998). The cellulose fibres dispersed in water tend to form aggregates, i.e. flocs, due to mechanical and non-mechanical factors, which has been studied experimentally for many years, e.g. Mason (1948), Norman *et al.* (1977) and Kerekes (1983). Furthermore the formation of the paper made in

a paper machine is dependent on the state of the fibre suspension flow in the forming section, i.e. the headbox and the former. In product development of pulp- and paper process equipment of today, the experimental work is combined with Computational Fluid Dynamics (CFD) modelling. For a cellulose fibre suspension in water, difficulties will arise with a multi-phase description due to the flexible long fibres and their many interactions with each other. Few attempts have been made to model fibre suspensions in turbulent flows, e.g. Andersson (1966), Hourani (1988*a*), Hourani (1988*b*), Steen (1989), and Steen (1990). The proposed model by Steen, i.e. the Fibre Flocculation Concept (FFC), for this complex system was based on a one-phase description of the fluid flow. In his model the fibrous phase is described only by the flocculation intensity solved as a passive scalar variable. The result of this approach is that the effects of the fibre phase on a main flow (i.e. average water flow and turbulence) are neglected. In the present paper the FFC by Steen will be investigated and compared to experimental data. The experimental data used was presented for a sudden enlargement of a circular pipe by Karema *et al.* (2001). This type of geometry can typically be found in a turbulence generator in a modern headbox for a paper- or board machine. The aim is to study the dilute consistency regime, i.e. ¡1%, that is expected in such equipment. The FFC is generally based on the governing equation for a general scalar fluctuation, e.g. Rodi (1993). The rupture term, i.e. the dissipation term, is similar to the one derived by Rodi but the aggregation terms, i.e. the production terms are different. The production of a scalar fluctuation is controlled by mean scalar gradients, while the flocculation aggregation in the FFC is based on that floc aggregation starts out as a small scale activation of fibres followed by floc collisions and fibre network settling, cf. Steen (1989), and Steen (1990).

2. Method

The numerical modelling work has been carried out with the commercial CFD code CFX5, ver. 5.5.1. All the simulations were turbulent, and the turbulent fluid flow was modelled with the standard k-e turbulence model, with the default values of the constants provided in the CFD code, cf. CFX (1999-2002). The geometry outline is the PPP3 reference geometry described in the paper by Karema *et al.* (2001). The geometry consists of a circular constriction block, which gives a contracting step and an expanding step respectively. The outer and inner diameters were 26 mm and 18.6 mm respectively. Fully developed inlet boundary conditions were set for all variables (velocity, turbulence and flocculation intensity) at the inlet of the PPP3 geometry. These boundary conditions were provided from CFD calculations of a straight long pipe, with the length to diameter ratio of 50. Further the PPP3 geometry was modelled as an axial-symmetric 2D case, with a structured discretization mesh. The total number of elements was 56850. For the near wall treatment, the so-called scalable wall function was used, cf. CFX (1999-2002). With the scalable wall function the predictions of the solution will be less sensitive to the choice of the point nearest to the wall. The flocculation intensity was solved as a passive

non-reacting scalar variable with the following general transport equation in the presence of turbulence.

$$\nabla \bullet (\rho \mathbf{U} \phi) - \nabla \bullet ((D_\phi + \frac{\nu_t}{Sc_t}) \nabla(\rho\phi)) = S_\phi \tag{1}$$

With the definition of flocculation intensity,

$$\phi = \frac{var(c)}{\overline{c}^2} = \frac{\overline{c'^2}}{\overline{c}^2} = \frac{c'^2_{rms}}{\overline{c}^2} \tag{2}$$

where, c', is the fluctuation in consistency, c'_{rms}, is the root-mean-square value and, $\overline{c}$, is the mean fibre consistency. This is defined analogous to the definition originally proposed by Wahren (1967), whereas he defines the intensity as the square root of equation (2). The effective diffusivity, D_{eff}, of the passive scalar is the sum of the kinematic diffusivity, D_ϕ, and the turbulent diffusivity, ν_t/Sc_t was set to 0.001 and the turbulent Schmidt number, Sc_t, was set to 0.9 according to the default value in the CFD code. The effective diffusivity will be further discussed in the results section. The source term includes both the rate of aggregation of flocs and rupture according to, cf. Steen (1989), and Steen (1990):

$$S_\phi = \rho(A - R) \tag{3}$$

The wall boundary condition for the flocculation intensity was set to zero at this tentative stage. The same constants presented by Steen (1990), were used for the flocculation intensity calculations. Exceptions made are the effective diffusivity, see discussion above, the fibre length and the fibre diameter. For the fibre properties, values were taken from Karema *et al.* (2001), i.e. the softwood kraft (pine), with average fibre length of 2.09 mm and average fibre diameter of 29.2 m.

3. Results

In Figure 1, measured floc volume and CCD images with its corresponding median threshold images can be seen for various locations downstream of the expanding step together with flocculation intensity simulations. The measurements were first presented by Houvila *et al.* (2000). The flocculation intensity contour plot, in Figure 1, is based on the present simulations with fully developed inlet conditions entering the step. The downstream position from the expanding step of the maximum turbulent kinetic energy for a circular-to-circular pipe expansion has its approximate location slightly upstream from the position of the re-attachment point for a pure fluid. In the experimental work by Karema *et al.* (2001), they showed that the maximum of the turbulent fluctuations of the fibrous phase and the minimum floc volume also coincide approximately with this location. Their measurement of the turbulent state of the fibrous phase was done with a pulsed ultrasound-Doppler anemometer. Also d'Incau (1989) clearly showed experimentally that the maximum strain

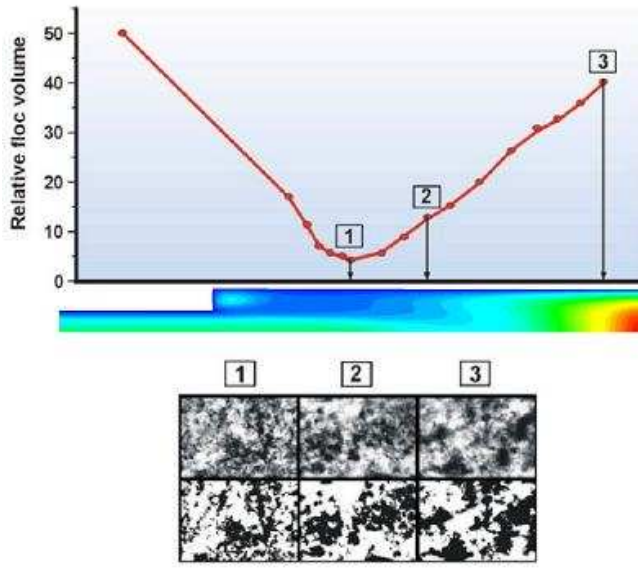

FIGURE 1. Floc volume, flocculation intensity and CCD images in a sudden circular pipe enlargement

rate and minimum macro length scale coincide at approximately the same position. The measured dimensionless floc volume for PPP3 geometry and for Pine at 0.5% consistency for different flow rates shows a decreasing minimum floc volume with increasing flow rate, cf. Figure 2, Karema *et al.* (2001). The same trend was found by Moayed (1999), measuring the flocculation intensity. The result of Karema et al. in Figure 2, also show how the curves seem to almost collapse into a common line independent of the flow rates from the point of minimum floc size and forward. CFD simulations were performed for the same geometry and flow rates as used by Karema et al. shown in Figure 2. The flocculation intensity values for the respective axial position were calculated as area weighted averages of the flocculation intensity field, cf. Figure 3. Also here the curves seems to collapse into a common curve. The minimum values are not that pronounced as in Figure 2, but the general trend is the same, i.e. increasing flow rate decreases the minimum value and vice versa. Furthermore the values tend to reach a saturation level for the respective flow rate. This type of saturation behaviour can be seen for another geometry with a smaller step and the same pulp, cf. Karema *et al.* (2001). No pronounced minimum after the step for the same geometry and low flow rates was also shown in the same paper for a birch pulp, i.e. shorter fibers. Further the figures clearly shows that the time scales differs, in the experimental data the flocs seem to grow at a slower rate than for the simulations. This still shows that even with the

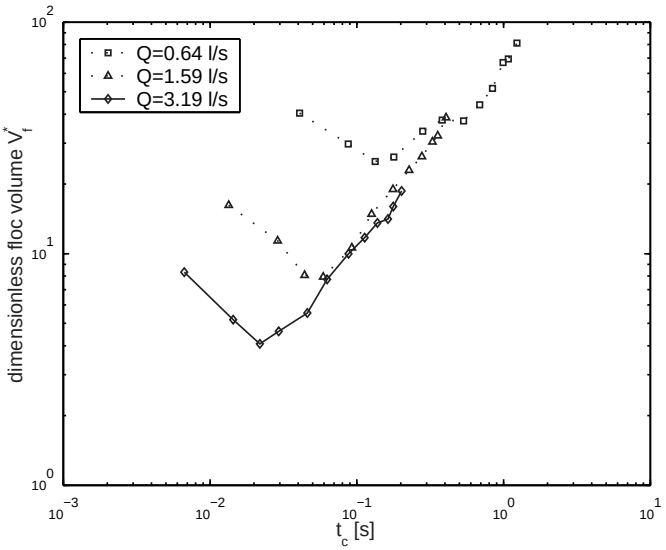

FIGURE 2. Dimensionless floc volume vs. mean residence time from the step, cf. Karema et al. (2001)

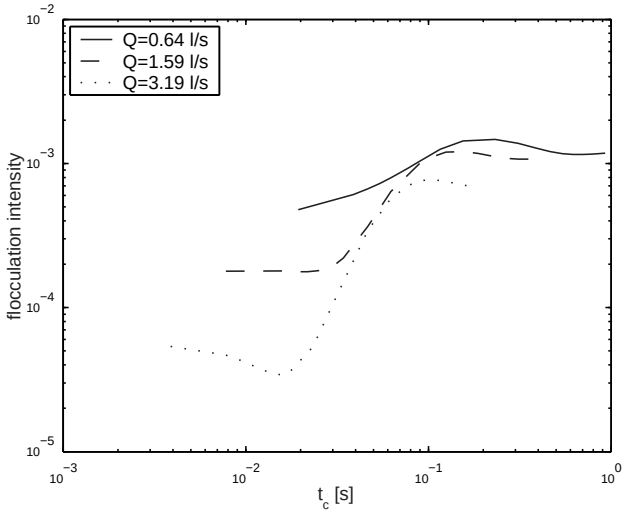

FIGURE 3. CFD simulated flocculation intensity as a function of mean residence time from the expansion

"non-tuned" FFC the simulations catch some of the physical behaviour. Using the minimum flocculation intensity/floc volume for the case of lowest flow rate

to normalise with the minima for the other flow rates, the two curves for normalised floc volume and flocculation intensity minima shows similar behaviour, cf. Figure 4. However the CFD simulations of the flocculation intensity tend to

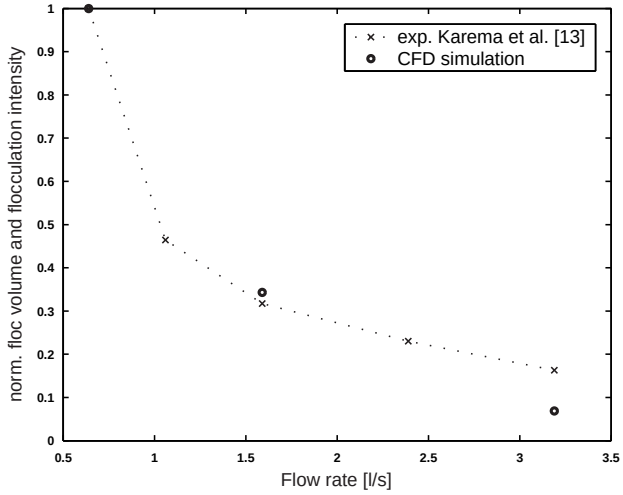

FIGURE 4. Normalized values of the floc volume and flocculation intensity vs. flow rate

be lower than the measured floc volume for the larger flow rates. The diffusivity term was varied, to be able to study the influence on the flocculation intensity profile, cf. Figure 5. The simulations were carried out for a flow rate of 1.59 l/s in a straight pipe with the inner diameter of 26 mm. In the paper by Steen (1990), the effective diffusivity was arbitrary set equal to 0.001. This includes both the kinematic and turbulent diffusivity when introduced in the equation for a passive non-reacting scalar variable in our case. For a fully developed fluid flow in a pipe the convective term vanishes. Therefore for vanishing effective diffusivity only the source term will be significant, and by setting this term equal to zero, i.e. $A = R$, it is possible to solve for a fully developed flocculation intensity profile in the case $D_{eff} = 0$, cf. Figure 5. The figure clearly shows how the presence of diffusivity to various degrees evens out the flocculation intensity profile. The various effective diffusivity models used are indicated in the legend of Figure 5. When decreasing the kinematic diffusivity the centre value, i.e. the peak value, goes asymptotically to a given value. This means that the diffusivity is dominated by turbulent diffusivity, cf. Figure 5 case $D_{eff} = 1.0 \cdot 10^{-5} + \nu_t/Sc_t$.

4. Conclusions

Even when using the "non-tuned" FFC it captures some general behaviour that is expected, thus prediction of a minimum after the step and the re-flocculation

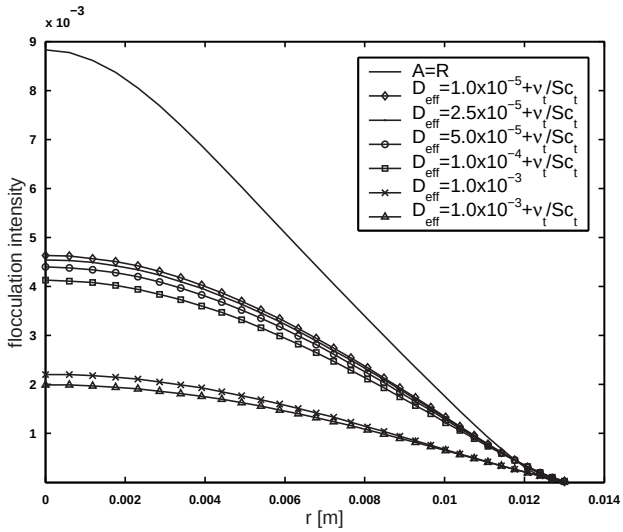

FIGURE 5. Effect with various effective diffusivities on the flocculation intensity profiles for a fully developed pipe flow

process. The curves for the re-flocculation process seem to collapse into a common curve, which is consistent with experimental data. The study also shows that in CFD simulations for increasing flow rate the minimum value of the measure of flocculation decreases at the same rate as experimental data, with an underestimation for the higher flow rates, cf. Figure 4. The CFD simulations and experimental data showed that the time scales differs. In the experimental data the flocs seem to grow at a slower rate than for the simulations. There is a need to determine the time constant for the FFC concept. The actual magnitude of the effective diffusivity term is also necessary to study further, cf. Figure 5. It is worth to point out here, that all the simulations for the fluid flow was described as single phase with no coupling from the fibrous phase. Therefore the re-attachment point was always underestimated for the simulation cases, which is a well-known inaccuracy of the standard k-e turbulence model and an effect of the non-coupling in momentum exchange between the phases. It is known that turbulence is influenced by the addition of fibres in water, e.g. Norman *et al.* (1977). Thus the use of this one-phase approach shows on a need of a modification of the turbulence model, which takes into account additional production and dissipation. There is a lack in literature of such modifications in turbulence for the presence of flexible long fibres. Still several articles on the interaction between particles and turbulence of the fluid phase have been published, e.g. Hestroni (1989) and Gore (1989). CFD modeling of a turbulent multi-phase flow is a challenging problem and all phenomena will be hard to capture in detail. But, even such a relatively simple model like the FFC, can predict flocculation tendency at least qualitatively correct.

Thus the model is a useful tool in R&D when studying the effect of headbox geometry and flow rate on flocculation and formation.

References

1999-2002 *CFX-5 and CFX-4 User Documentation*. AEA Technology plc.

Andersson, O. 1966 Some observation on fibre suspensions in turbulent motion. *Svensk Papperstidning* **69(2)**, 23–31.

Andersson, O. & Steen, I. 1962 Non-uniformity on sheet structure. In *Transactions of the Symposium held at Oxford: 1962*, , vol. 1(2), pp. 771–789.

d'Incau, S. 1989 Characteristic of the decay of turbulence in a pulp suspension flow. *International Journal of Multiphase Flow* **15(5)**, 735–746.

Gore, R. A. 1989 Effect of particle size on modulating turbulent intensity. *International Journal of Multiphase Flow* **15(2)**, 279–285.

Hestroni, G. 1989 Particle-tubulence interaction. *International Journal of Multiphase Flow* **15(5)**, 735–746.

Hourani, M. 1988*a* Fiber flocculation in pulp suspension flow part1: Theoretical model. *Tappi Journal* pp. 115–118.

Hourani, M. 1988*b* Fiber flocculation in pulp suspension flow part2: Experimental results. *Tappi Journal* pp. 186–189.

Houvila, J., Lepomäki, H., Lumiala, J. & Kirvesmäki, J. 2000 The valmet headbox family-a new level of customer orientation. In *Valmet Paper Technology Days 2000, Turku, Finland*.

Karema, H., Salmela, J., Tukiainen, M. & Lepomäki, H. 2001 Prediction of paper formation by fluidisation and reflocculation experiments. *12th Fundamental Research Symposium* pp. 559–589.

Kerekes, R. 1983 Flocculation in decaying turbulence: A literature review. *J. Pulp Paper Sci.* pp. TR86–TR91.

Mason, S. G. 1948 The flocculation of cellulose fibre suspensions. *Pulp and Paper Magazine of Canada* pp. 99–104.

Moayed, R. 1999 Characterization of fibre suspension flows at papermaking consistencies. PhD thesis, Department of Chemical Engineering and Applied Chemistry, University of Toronto, 1999, Toronto, Canada.

Norman, B. 1998 *Papermaking Science and Technology, Ch.6, Book 8(19)*. Fapet OY.

Norman, B., Möller, K., Ek, R. & Duffy, G. 1977 Hydrodynamics of papermaking fibres in water suspension. In *Fibre - Water Interactions in Papermaking: Transactions of the Symposium held at Oxford: September 1977*, , vol. 1(2), pp. 195–249.

Norman, B. & Söderberg, D. 2001 Overview of forming literature, 1990-2000. *Trans. 12th Fundamental Research Symposium, Oxford* **1**, 431–558.

Norman, B. & Wahren, D. 1972 A comprehennsive method for the description of mass distribution in sheet and flocculation and turbulence in suspensions. *Sv. Papperstidning* **75(20)**, 807–818.

Rodi, W. 1993 *Turbulence Models and Their Application in Hydraulics A State-of-the-art review*, 3rd edn. IAHR-AIRH, A.A.Balkema, Rotterdam.

Steen, M. 1989 A concept for fibre flocculation in turbulent flow. *The 9th Fundamental Research Symposium, Cambridge, UK* pp. 251–274.

Steen, M. 1990 Modelling fibre flocculation in turbulent flow; a numerical study. *TAPPI Engineering Conference, Seattle, USA* pp. 475–486.

Wahren, D. 1967 Proposed definitions of some basic papermaking terms. *Sv. Papperstidning* **70(21)**, 725.

Paper 2

2

A Numerical Study on Mechanical Fibre Flocculation in a Planar Contraction

By Marko Hyensjö[1,2] & Anders Dahlkild[2]

[1]Metso Paper Karlstad AB, P.O. Box 1014, SE-651 15 Karlstad, Sweden
[2]FaxénLaboratoriet, KTH, SE-100 44 Stockholm, Sweden

To be submitted

The flocculation behavior in a planar contraction is studied numerically. Two fibre flocculation models in the literature have been implemented and reviewed, namely the Fibre Flocculation Concept (FFC) introduced by Steen versions 1990 and 1993 respectively. Moreover various turbulence models is studied in conjunction with the fibre flocculation models. The result reveals large differences in the magnitude of the flocculation intensity between the two flocculation models. Starting at an equilibrium between aggregation and rupture the later model, FFC-1993, gives lower magnitude of flocculation intensity. Since the fibre flocculation model uses the turbulent quantities, such as k and ε, is the numerical prediction of these is a crucial feature. The standard $k-\varepsilon$ turbulence model will predict an un-physical behavior of the normal stress, in the direction of the contraction, and therefore also predict an un-physical fibre flocculation. The Reynolds Stress turbulence models gives a better qualitative prediction of the turbulence quantities than the isotropic standard $k-\varepsilon$ turbulence model. Fibre properties, i.e. fibre length and diameter, will by comparison predict different behavior of flocculation intensity evolution in a planar contraction with FFC-1990 for typical headbox flows. Longer fibres are activated easier and from an equilibrium state at the inlet the flocculation intensity increases throughout the contraction. A shorter fibre such as birch will predict the opposite. In addition both long and short fibres will give an increase in flocculation intensity starting from a non-equilibrium state at low intensity. This trend is supported in experimental result from the literature.

1. Introduction

Cellulose fibres dispersed in water tend to form aggregates, i.e. flocs, due to mechanical and nonmechanical factors, studied experimentally by e.g. Mason (1954), Norman *et al.* (1977) and Kerekes (1983). The state of these aggregates in the forming section, i.e. the headbox and the former, of a papermachine determines the formation of the final paper made. For a numerical modelling of a cellulose fibre suspension in water, difficulties will arise with a multi-phase description due to the flexible long fibres and their many interactions with each

other. Few studies are reported in the literature to model fibre suspensions in turbulent flows, e.g. Andersson (1966) , Hourani (1988*a*), Hourani (1988*b*), Steen (1990), Steen (1993), Plikas *et al.* (2000), Kuhn & Sullivan (2001) and Hyensjö *et al.* (2003). The model proposed by Steen, i.e. the Fibre Flocculation Concept (FFC), is based on a one-phase description of the fluid flow. In his model the fibrous phase is only described by the flocculation intensity solved as a passive scalar variable. The result of this approach is that the effects of the fibre phase on a main flow (i.e. average water flow and turbulence) are neglected. The FFC is based on the governing equation for a general scalar fluctuation, e.g. Rodi (1993). The rupture term, i.e. the dissipation term, is similar to the one derived by Rodi (1993) but the aggregation term, i.e. the production term is different. The production of a scalar fluctuation is usually controlled by mean scalar gradients, while the flocculation aggregation in the FFC is based on that floc aggregation starts out as a small scale activation of fibres followed by floc collisions and fibre network settling, cf. Steen (1990) and Steen (1993). In the work by Plikas *et al.* (2000) and Kuhn & Sullivan (2001), a similar analogy with a general scalar fluctuation is used. However both dissipation and production terms are based on model constants which are calibrated against experimental data by Moayed (1999). This makes it applicable only for that particular grid-generated turbulence flow cell.
In the present paper the FFC by Steen is investigated in a planar contraction, which is a typical geometry in a headbox just before the free jet. Two slightly different versions of FFC is reported named here as FFC-1990 and FFC-1993, cf. Steen (1990) and Steen (1993). Results from these two versions are presented and the difference of them are discussed. Various parameters, e.g. fibre properties, i.e. fibre length and diameter, flow rate and the state of the fibre suspension is considered and studied. Furthermore the aim is to study the dilute consistency regime, i.e. <1%, which is expected in papermaking.

2. The Fibre Flocculation Concept - FFC

The flocculation intensity, ϕ, in FFC is solved as a passive non-reacting scalar variable with the following general steady state transport equation:

$$\nabla \bullet (\rho \mathbf{U} \phi) - \nabla \bullet (\Gamma_\phi \nabla(\rho\phi)) = S_\phi \tag{1}$$

with the definition of flocculation intensity, ϕ,

$$\phi = \frac{var(c)}{\overline{c}^2} = \frac{\overline{c'^2}}{\overline{c}^2} = \frac{c'^2_{rms}}{\overline{c}^2} \tag{2}$$

where, c', is the fluctuation in consistency, c'_{rms}, is the root-mean-square value and, $\overline{c}$, is the mean fibre consistency. This is defined analogous to the definition originally proposed by Wahren (1967), were the intensity is defined as the square root of the right hand side of equation (2). Γ_ϕ is the effective diffusivity of the passive scalar which for the original FFC was set to an arbitrary value of 0.001. For a true turbulent case it includes both the kinematic diffusivity and

the turbulent diffusivity. Hyensjö *et al.* (2003), study the effect of various effective diffusivity values on the flocculation intensity profile for a fully developed pipe flow with FFC-1990. The source term, S_ϕ, includes both aggregation of flocs and rupture which will be discussed further in the following sections. It is mainly the source term that differs between the two version available, FFC-1990 and FFC-1993. Furthermore since the source term for FFC describes the main action concerning the flocculation process, this is the foremost feature for a successful flocculation model. In FFC the turbulence fluctuations are divided into large scales and small scales. The intensity of the large scales are expressed for the isotropic turbulence case as the root-mean-square value of the turbulence fluctuations:

$$u'_{rms} = \sqrt{\frac{2k}{3}} \tag{3}$$

The small scales are the Kolmogorov scales in the flow and the velocity and length scales, are expressed as:

$$u^* = 1.74(\nu\varepsilon)^{1/4},\ l^* = 1.43(\frac{\nu^3}{\varepsilon})^{1/4} \tag{4}$$

In FFC the ratio of the velocity scales, $\gamma = u^*/u'_{rms}$, defines the volumetric fraction of the fine structure region and $(1-\gamma)$ defines the fraction of the large scale region. The FFC postulates moreover that the large scale region, $(1-\gamma)$, will contain flocs and in the fine structure region, γ, there will only be single fibres. Therefore the average consistency in the large scale region, i.e the floc consistency, is defined as:

$$c_{floc} = \overline{c} + c'_{rms} \tag{5}$$

Furthermore the definition of the mean consistency is expressed in terms of the average fiber consistencies in respective region as:

$$\overline{c} = c_{floc}(1-\gamma) + c^*\gamma \tag{6}$$

where c^* is the consistency of the fine structure region. The mean consistency in the FFC is either prescribed to a constant, homogenous value, or calculated from an average conservation equation for the fibrous phase. The root mean square of the fibre consistency fluctuations, c'_{rms}, is given by the solution of equation (2), and equation (6) then defines the value of c^*.

2.1. *The Fibre Flocculation Concept - 1990*

The source term, S_ϕ, has the following definition for the FFC-1990, cf. Steen (1990), which includes both aggregation, A, and rupture, R, of flocs:

$$S_\phi = \rho(A - R) \tag{7}$$

The rupture term, R, is based on the analogy to the turbulent energy cascade where a passive scalar under assumptions of isotropic and homogeneous turbulence can be modelled as:

$$R = C_{f2}\frac{\varepsilon}{k}\phi \tag{8}$$

The constant, C_{f2} is a constant, specifying the ratio of the time scale characterizing the scalar fluctuation to that characterizing the velocity fluctuation, cf. Rodi (1993). This can vary from 1 to 2 depending on the flow considered, cf. Launder (1977). In the FFC, C_{f2}, is set to 1. Now, aggregation is supposed to be a result of collisions between the free fibres in the fine structure regions and flocs in the large structure regions. The aggregation, A, may then be written as the product of three factors, $A1$, $A2$ and $A3$, representing different physical effects. Firstly, the average probability of collisions is proportional to the product of the respective average volumetric concentrations of free fibres, γc^*, and flocs, $(1-\gamma)c_{floc}$. Thus

$$A1 = \gamma c^*(1-\gamma)c_{floc} \tag{9}$$

Secondly, the rate of aggregating collisions is assumed proportional to the inverse of the Kolmogorov time scale, $1/\tau = u^*/l^*$, and the resonance energy transfer coefficient, $f(\frac{\omega}{\omega_0})$. Then,

$$A2 = \frac{u^*}{l^*}f(\frac{\omega}{\omega_0}) \tag{10}$$

where

$$f(\frac{\omega}{\omega_0}) = \frac{(\frac{\omega}{\omega_0})^2}{((1-(\frac{\omega}{\omega_0})^2)^2 + \beta^2(\frac{\omega}{\omega_0})^2} \tag{11}$$

with

$$\omega = \frac{u^*}{l^*}, \omega_0 = \sqrt{\frac{4EI}{\rho d^2 l^4}} \tag{12}$$

where l is the fiber length and d, the fiber diameter, EI, the stiffness of a fiber, and β, damping factor. At last a factor A3 accounts for a finite settling time , t_{fib}, for a free or surface fibre of a floc after collision. If t_{fib} is longer than a typical floc-fibre contact time, t', estimated by the time scale of the largest eddies, k/ϵ, then the collision is less efficient. Therefore,

$$A3 = \frac{t'}{t_{fib}} \approx \frac{k}{\varepsilon}\frac{1}{t_{fib}} \tag{13}$$

The complete aggregation term, A, is then expressed as:

$$A = C_{f1}\frac{1}{\bar{c}^2}A1A2A3 \tag{14}$$

where C_{f1} is set to 1. Now making equation (1) dimensionless by dividing with $\rho U_0/L$. Motivation for this is to find out the dependent variables for the dimensionless aggregation and rupture term. This gives the dimensionless source term, S'_ϕ,

$$S'_\phi = \frac{S_\phi}{\frac{\rho U_0}{L}} = \frac{\rho(A-R)}{\frac{\rho U_0}{L}} \tag{15}$$

scaling now k with U_0^2 and ε with U_0^3/l_ε, where l_ε is the dissipative length scale, giving,

$$\widetilde{k} = \frac{k}{U_0^2},\ \widetilde{\varepsilon} = \frac{\varepsilon l_\varepsilon}{U_0^3} \tag{16}$$

The inlet boundary conditions,

$$k_0 = \frac{U_0^2(T_{u0}^2 + T_{v0}^2 + T_{w0}^2)}{2} = \frac{3U_0^2\overline{T}_0^2}{2},\ \varepsilon_0 = \frac{k_0^{\frac{3}{2}}}{l_\varepsilon} \tag{17}$$

and in dimensionless form,

$$\widetilde{k_0} = \frac{3\overline{T}_0^2}{2},\ \widetilde{\varepsilon}_0 = \widetilde{k}_0^{\frac{3}{2}} \tag{18}$$

where $\overline{T}_0$ is the average turbulence intensity. Equation (18) shows that the dimensionless inlet turbulent quantities is only a function of the average turbulence inlet intensity. The rupture term, R, in dimensionless form will furthermore be,

$$\frac{\rho R}{\rho\frac{U_0}{L}} = C_{f2}\frac{\widetilde{\varepsilon}}{\widetilde{k}}\frac{U_0^3}{l_\varepsilon}\frac{1}{U_0^2}\frac{L}{U_0}\phi = C_{f2}\frac{\widetilde{\varepsilon}}{\widetilde{k}}\frac{L}{l_\varepsilon}\phi \tag{19}$$

This gives the inlet dimensionless Rupture term,

$$\widetilde{R}_0 = C_{f2}\widetilde{k}^{\frac{1}{2}}\frac{L}{l_\varepsilon}\phi_0 = C_{f2}\sqrt{\frac{3}{2}}\overline{T}_0\frac{L}{l_\varepsilon} \tag{20}$$

Showing that the inlet dimensionless rupture term is dependent on the turbulence intensity at the inlet and the dissipative length scale. Now the aggregation term can be rewritten with Equations (2), (6) and (14) as,

$$\rho A = \rho C_{f1}[1-(1-\gamma)(1+\sqrt{\phi}](1-\gamma)(1+\sqrt{\phi})]f(\frac{\omega}{\omega_0})\frac{1.74}{1.43}(\frac{\varepsilon}{\nu})^{\frac{1}{2}}\frac{k}{\varepsilon}\frac{1}{t_{fib}} \tag{21}$$

or

$$\rho A = \rho C_{f1}[1-(1-\gamma)(1+\sqrt{\phi}](1-\gamma)(1+\sqrt{\phi})]f(\frac{\omega}{\omega_0})\frac{1.74}{1.43}\frac{k}{\sqrt{\nu\varepsilon}}\frac{1}{t_{fib}}. \tag{22}$$

Furthermore the following observation can be made, i.e.,

$$\gamma^2 = \frac{u^{*2}}{u'^2_{rms}} = \frac{3}{2}1.74^2\frac{\sqrt{\nu\varepsilon}}{k} = \frac{3}{2}1.74^2\frac{\sqrt{\nu\frac{U_0^3}{l_\varepsilon}}}{U_0^2}\frac{\sqrt{\widetilde{\varepsilon}}}{\widetilde{k}} = \frac{3}{2}1.74^2\sqrt{\frac{\nu}{U_0 l_\varepsilon}}\frac{\sqrt{\widetilde{\varepsilon}}}{\widetilde{k}} \tag{23}$$

Now, defining a Reynolds number based on the dissipative length scale,

$$Re_{l_\varepsilon} = \frac{U_0 l_\varepsilon}{\nu} \tag{24}$$

the dimensionless aggregation term together with Equations (22), (23), and (24) gives,

$$\frac{\rho A}{\frac{\rho U_0}{L}} = \rho C_{f1}[1-(1-\gamma)(1+\sqrt{\phi}](1-\gamma)(1+\sqrt{\phi})]f(\frac{\omega}{\omega_0})\frac{1.74}{1.43}\sqrt{Re_{l_\varepsilon}}\frac{\widetilde{k}}{\sqrt{\widetilde{\varepsilon}}}\frac{L}{U_0 t_{fib}} \tag{25}$$

Equation (25) shows that the dimensionless aggregation term is dependent on velocity as $1/\sqrt{U_0}$. Note also that the function f is dependent on the Kolmogorov scales. $\omega = u^*/l^*$.

2.2. *The Fibre Flocculation Concept - 1993*

The source term for the FFC-1993 version is defined as follows, cf. Steen (1993):

$$S_\phi = A - \rho R \tag{26}$$

where the rupture term, R, has the same definition as in equation (8). Note that now the aggregation term is not multiplied with the density, ρ, cf. equation (7). The aggregation term on the other hand is modified to be:

$$A = C_7 \frac{1}{\overline{c}^2}(\frac{l}{d})^2 A1A2A3 \tag{27}$$

The constant, C_7, is set to be 1E-3. The term $A1$ is now:

$$A1 = \gamma c^*(1-\gamma)(c_{floc} - c^*) = c^*(1-\gamma)c'_{rms} \tag{28}$$

which differs from FFC-1990 by the second factor, cf. equation (9). The floc consistency, $\overline{c} + c'_{rms}$, is now reduced by the fine structure consistency, c^*. Furthermore in the $A2$ term the resonance energy transfer coefficient, cf. equation (11), is not allowed to be lower than $1/\beta^2$, when $\omega^* > \omega_0$. The $A3$ term is similar to that in FFC-1990, cf. equation (13).

2.3. *Summary of the Fibre Flocculation Concept*

There are four differences between FFC-1990 and FFC-1993. Firstly in the source term the density is not multiplied with the aggregation term, cf. equations (7) and (26). This will in a closer look lead to inconsistency with units. Secondly, disregarding this fact, the aggregation term has decreased 100 times in magnitude. This by comparing equations (7),(14),(26) and (27) and using $l = 3mm$ and $d = 30\mu m$. Thirdly in equation (28), the A1 factor is proportional to the intensity of the consistency fluctuations, c'_{rms}. This can be interpreted that with no variation in consistency there will be no aggregation. Moreover since A1 in both FFC-1990 and FFC-1993 is proportional to fine structure consistency, c^*, the aggregation term will vanish if all the fibres are located in the large scale region as flocs, i.e. if c^* is zero. Fourthly the resonance energy transfer coefficient which is a distribution function with maximum at resonance frequency, is restricted to a value of $1/\beta^2$, for frequencies higher than, ω_0. This

is motivated with that other eddies in the turbulent structure may be able to activate fibres for $\omega^* > \omega_0$.

3. Method

The numerical modelling work has been carried out with the commercial CFD code CFX5, ver. 5.5.1. The flow was modelled with three different turbulence models, the standard k-ε model, the Reynolds Stress model (LLR-IP) and the Omega-Reynolds Stress model (SMC-ω) with default values of the constants provided in the CFD code, cf. CFX (1999-2002). Exception made for the dissipation length scale, which has been varied for the k-ε model, see further results section. The geometrical outline modelled is provided from the work by Parsheh (2001). The geometry is due to symmetrical reasons modelled as the upper half of a planar contraction, cf. Figure 1.

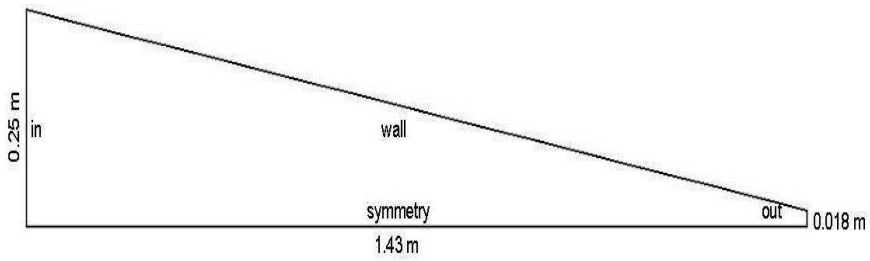

FIGURE 1. The geometrical outline, cf. Parsheh (2001), modelled as a half planar contraction (Note: Out of scale.)

For the near wall treatment, the so-called scalable wall function was used, cf. CFX (1999-2002). The structured grid has 100 elements in height and 500 elements along the channel length and 1 element in the depth. The density $\rho = 998kg/m^3$ and the dynamic viscosity $\mu = 1 \cdot 10^{-3}kg/ms$. Inlet boundary conditions for the velocity components were set to, $U_0 = 0.18m/s$, $W_0 = 0$ and potential flow was considered for V_0 giving:

$$V_0 = \frac{2Q\tan\theta}{(2L\tan\theta + h)^2}y \tag{29}$$

Here Q, is the flow rate, θ, the half angle of the contraction, L, the length of the contraction and, h, the height of the contraction. These settings gives an outlet velocity of 2.5 m/s, which corresponds to a headbox jet speed of 150 m/min. Studies are also made for typical headbox flows, giving jet speeds of 1000, 1500 and 2000 m/min. For the inlet boundary conditions of the turbulent quantities k_0 and ε_0, the turbulent intensity, $T_{u0} = 3.6\%$, $T_{v0} = 3.8\%$ and $T_{w0} = 3.5\%$,

measurements by Parsheh (2001) were used (case C14gl, $C = 13.8$):

$$k_0 = \frac{U_0^2(T_{u0}^2 + T_{v0}^2 + T_{w0}^2)}{2},\ \varepsilon_0 = \frac{k_0^{3/2}}{l_\varepsilon} \tag{30}$$

The above values for turbulence intensities was used in most of the cases in results section if nothing else is specified. The inlet flocculation intensity value, ϕ_0, was obtained from the aggregation term, A, set equal to the rupture term, R, with given k_0 and ε_0, which corresponds to a fully developed flocculation field with a vanishing convective term, and with the effective diffusivity term neglected. In view of the fact that the single phase velocity field is not fully developed at the contraction inlet this assumption is a simplification of the true conditions which are not known. Two different wall boundary conditions have been studied for the flocculation intensity namely zero value, $\phi = 0$, and zero gradient, dϕ/dn=0. For FFC-1990 and FFC-1993 the following values has been used; l= 3mm, $d = 30\mu m$, $t_{fib} = 1s$, $\beta = 10$, $C_{f1} = 1$, $C_{f2} = 1$, $C_7 = 1 \cdot 10^{-3}$, and $EI = 1 \cdot 10^{-12} Nm^2$. The effective diffusivity, Γ_ϕ, includes both the kinematic diffusivity, Γ_k, and the turbulent diffusivity, Γ_t, according to:

$$\Gamma_\phi = \Gamma_k + \Gamma_t = \Gamma_k + \frac{\nu_t}{Sc_t} \tag{31}$$

Γ_k is set to $0.001 m^2/s$. Sc_t corresponds to the turbulent Schmidt number which is set to 0.9 according to the default value in the CFD code. The definition of the kinematic eddy viscosity, ν_t, is dependent on the turbulence model applied, cf. CFX (1999-2002). In FFC-1990 and FFC-1993 an even mean consistency is assumed.

4. Results

Measured, by Parsheh (2001), and modelled normal components of the Reynolds Stresses along the centerline of a planar contraction is shown in Figure 2. The local contraction ratio, C, is defined as:

$$C = \frac{U}{U_0} \tag{32}$$

where U is the local velocity along the centerline and U_0 is the inlet velocity. The normal component of the Reynolds Stress in the x-direction, the direction along the contraction, shows a good prediction. The other two components fails in prediction. Similar results is shown by Parsheh (2001), using an algebraic Reynolds Stress and differential Reynolds Stress models. Development of the turbulent kinetic energy along the contraction centerline normalized by the inlet values for different turbulence models compared with experimental data provided by Parsheh (2001), is shown in Figure 3. The turbulence models compared are the standard k-ε model, the Reynolds Stress model (LLR-IP) and the Omega-Reynolds Stress model (SMC-ω). Additionally the standard k-ε model is computed with two different dissipative length scales, which provides

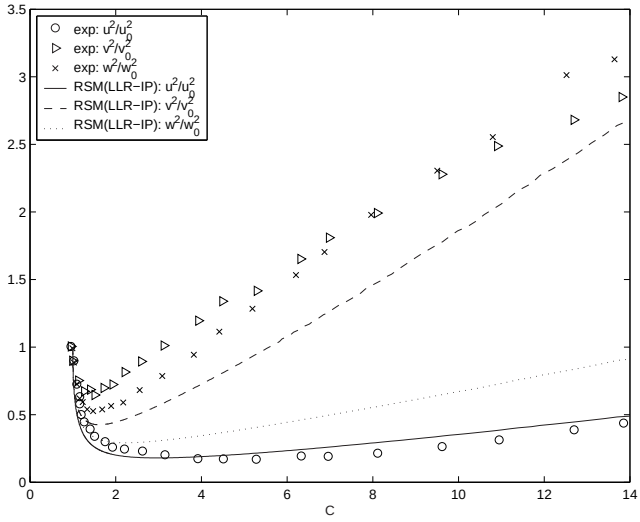

FIGURE 2. Measured, by Parsheh (2001), and modelled normal components of the Reynolds Stresses along the centerline of a planar contraction

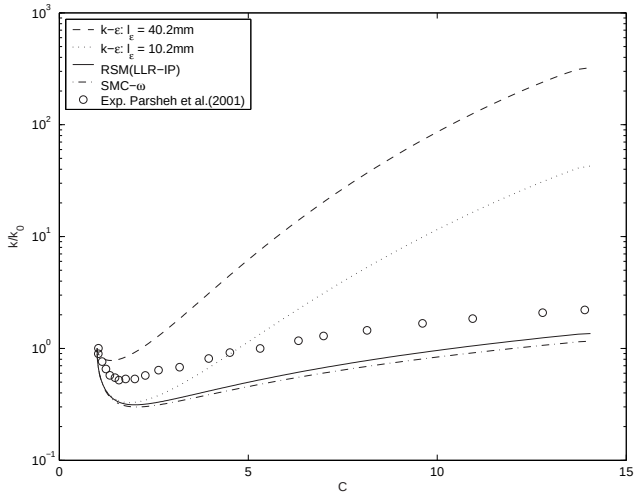

FIGURE 3. Turbulent kinetic energy normalized with inlet value for different turbulence models compared with experimental data provided by Parsheh (2001)

separate inlet boundary conditions for k and ε. To achieve a good prediction Parsheh (2001) demonstrates the importance of choosing a appropriate dissipative length scale for a Reynolds Stress model and a Algebraic Reynolds

Stress model. A decrease of the dissipative length scale will restrain the turbulent components. The Reynolds Stress models are modeled with a dissipative length scale of 10.2mm. The commercial code, CFX, recommends to use 0.3 times a typical length scale, which can be for example the hydraulic diameter or mesh size. Furthermore in Figure 3, the Reynolds Stress models seems to give a better qualitative agreement with experimental data. Figure 4 reveals a

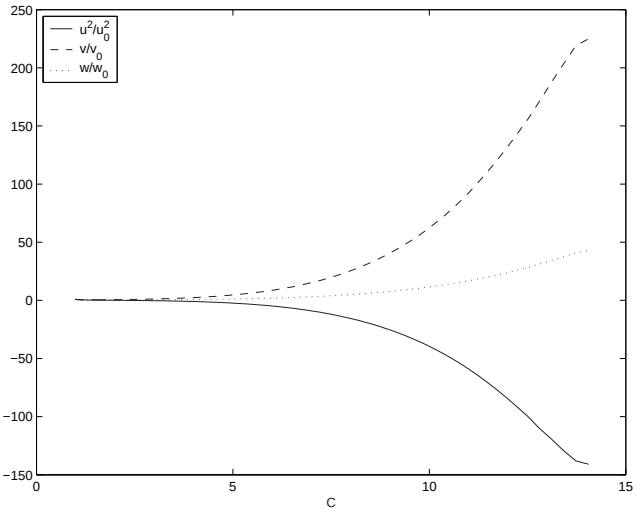

FIGURE 4. Turbulent normalized components along the contraction line modeled with the k-ε turbulence model

background as to why the k-ε turbulence model fails to predict the turbulent component in such flows. In a flow with a high rate of strain the k-ε model will overstress k and v^2, which will lead to a negative u^2, cf. Parsheh (2001), where the different normal stresses are evaluated according to:

$$\overline{u^2} = \frac{2}{3}k - \upsilon_t(2\frac{\partial U}{\partial x}) \tag{33}$$

$$\overline{v^2} = \frac{2}{3}k + \upsilon_t(2\frac{\partial U}{\partial x}) \tag{34}$$

$$\overline{w^2} = 2k - \overline{u^2} - \overline{v^2} = \frac{2}{3}k \tag{35}$$

The evolution of flocculation along the centerline in a planar contraction is here quantified with the normalized flocculation intensity, ϕ/ϕ_0 ($\phi_0 = 3.57 \cdot 10^{-3}$), cf. Figure 5. Two different turbulence models with FFC-1990 are compared, the k-ε and the Reynolds Stress model (LLR-IP). Also for the Reynolds Stress model two different boundary conditions for the flocculation intensity, ϕ, are tested, zero value, $\phi = 0$, and zero gradient at the wall. As can be seen the k-ε

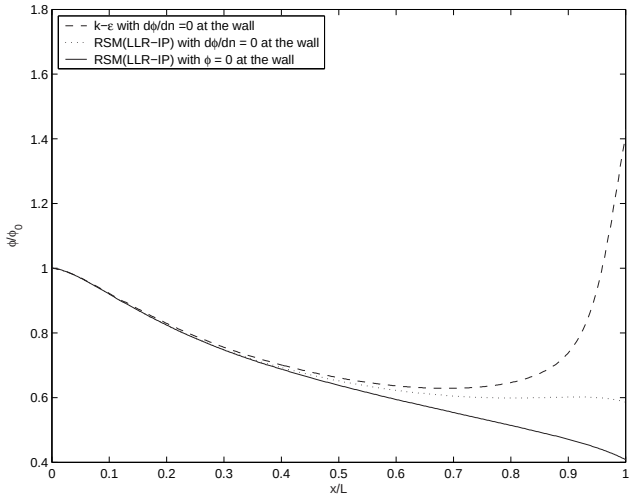

FIGURE 5. Normalized flocculation intensity with inlet value along centerline of the contraction for different turbulence models with FFC-1990

turbulence model will give a non physical behavior of the flocculation intensity development due to factors described earlier. The Reynolds Stress Model (LLR-IP) gives a more intuitive description of the flocculation behavior in a planar contraction. The outlet value of the flocculation intensity is dependent on which boundary condition for ϕ that is chosen. The case with isolated wall boundary condition, dϕ/dn=0, gives the highest flocculation intensity outlet level. This due to the fact that the quantity, ϕ, is globally preserved in the planar contraction. In Figure 6 normalized flocculation intensity ($\phi_0 = 3.57 \cdot 10^{-3}$) outlet profiles of the contraction for the two different boundary conditions is shown. As can be seen the profiles have the same shape but the case with dϕ/dn=0, is shifted towards higher values. The result from the two versions, FFC-1990 and FFC-1993, are shown in Figure 7. These simulations are made with the RSM (LLR-IP) turbulence model and with dϕ/dn=0 at the wall and an even mean consistency is assumed for both FFC-1990 and FFC-1993. The difference in result for the equilibrium inlet of the flocculation intensity between the versions are striking. The flocculation intensity at the inlet $\phi_0 = 2.39 \cdot 10^{-9}$ for FFC-1993 which is six orders of magnitude lower that for the FFC-1990. This is partly a result of the fact that the aggregation term includes a factor 100 times smaller in FFC-1993 than FFC-1990, cf. equations (7), (14), (26), and (27). This will give a lower level of equilibrium for the equations. The normalized flocculation intensity, ϕ/ϕ_0, has qualitatively the same behavior in the two cases, although FFC-1993 gives values below that of FFC-1990. The signification of the local equilibrium state, $A = \rho R$ for FFC-1993, is illustrated

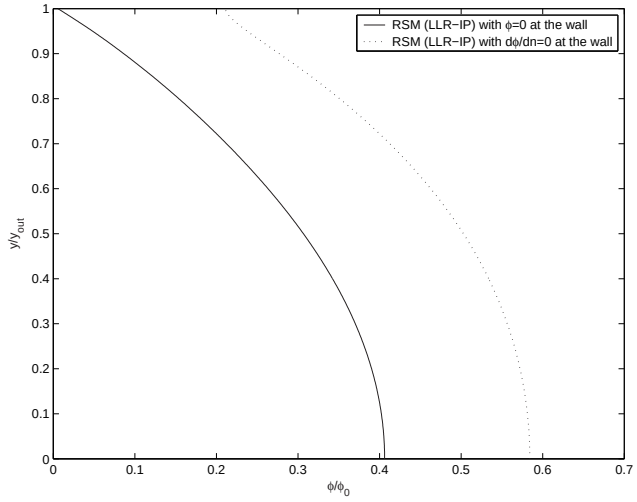

FIGURE 6. Contraction outlet profiles of the flocculation intensity for different wall boundary conditions for ϕ, with FFC-1990

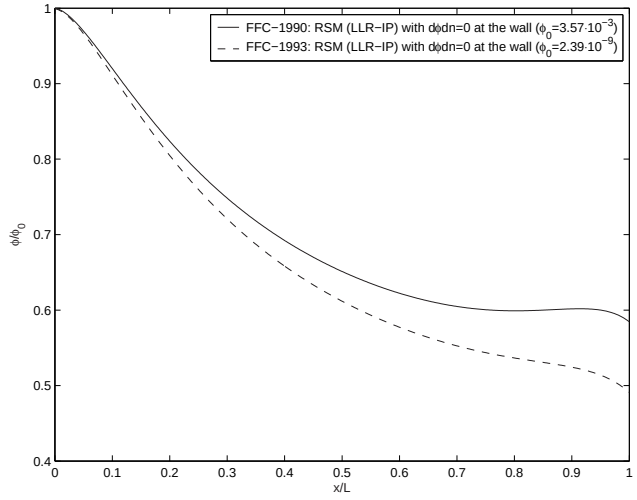

FIGURE 7. Normalized flocculation intensity with inlet value along centerline of the contraction for the two different versions FFC-1990 and FFC-1993

in Figure 8. When solving for $A = \rho R$ along the contracting the convective and diffusive terms are neglected. The solution is allowed to find a local equilibrium for a value of the normalized flocculation intensity, ϕ/ϕ_0 ($\phi_0 = 2.39 \cdot 10^{-9}$), in every position along the contraction. Now, the full solution of FFC-1993

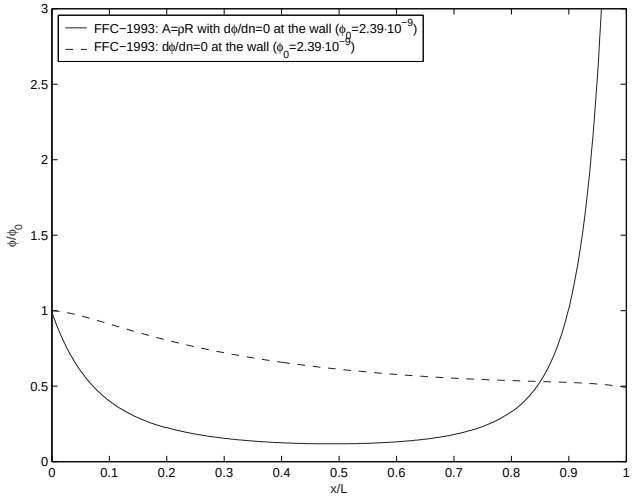

FIGURE 8. The significance of the convective and diffusive term along the contraction for FFC-1993

shows the significance of including convective and diffusive terms. Thus, the flocculation process is far from being at equilibrium along the contraction. The discrepancy is largest in the final part of the contraction were the velocity acceleration is dominating. The development of the source term, S_ϕ, along the contraction centerline for FFC-1993 and RSM(LLR-IP) turbulence model is shown in Figure 9. In the beginning there is a negative value, i.e. the source term is rupture dominating cf. equation (26). This is also illustrated in Figure 7, where the normalized flocculation intensity is decreasing. At a x/L value of about 0.84 the source term is shifted to be dominated by aggregation. In Figure 7 this can be seen that the gradient is decreasing towards the region of x/L values of about 0.8 to 0.9. The effect of the rapid increase of the source term is not seen in Figure 7. This is a consequence of the increased turbulence generated close to the wall in vicinity of the outlet accelerating channel were the rupture term will be dominated. This will effect the centerline even though the source term is positive. The effect of increasing or decreasing magnitude of the source term for FFC 1990 is illustrated in Figure 10. As the magnitude of the source term is increased will this drive the solution to the equilibrium state, i.e. Aggregation equals Rupture (A=R). The opposite with decreasing magnitude of the source term gives a trend towards the solution of S=0, i.e. flocculation intensity value preserves with the value of unity for the case with dϕ/dn=0 at the wall. The inlet value of the flocculation intensity has been chosen in earlier figures to be at equilibrium state with the inlet turbulence quantities k_0 and ε_0. In a real headbox contraction will this not most likely be the case. In experimental work by Karema *et al.* (2001) a sudden pipe expansion is considered and equilibrium state is achieved further downstream

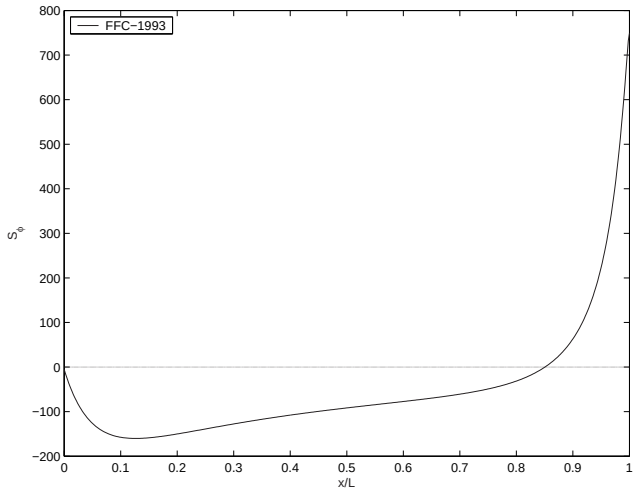

FIGURE 9. The development of the source term along the centerline of the contraction with FFC-1993 and RSM(LLR-IP) turbulence model

of the step than the length of a typical turbulence generator secondary tube. On the other hand the result by Karema *et al.* (2001) demonstrates that a longer Pine fibre in combination with a smaller step, then equilibrium state is achieved faster. This is to be taken into careful consideration when studying specific cases. Varying the magnitude of the inlet value of the flocculation intensity will give different result of the evolution of the flocculation intensity through out the contraction, cf. Figure 11. For a non-equilibrium state there will be a increase of the flocculation intensity instead of the decrease shown in a equilibrium case. With a almost homogenous fibre suspension, i.e. low flocculation intensity value of $0.01\phi_0$ there will be a continuously increase of the flocculation intensity value with the most rapid increase in the beginning of the contraction. Now comparing FFC-1990 and FFC-1993 for the same case is the difference in result striking, cf. Figure 12.

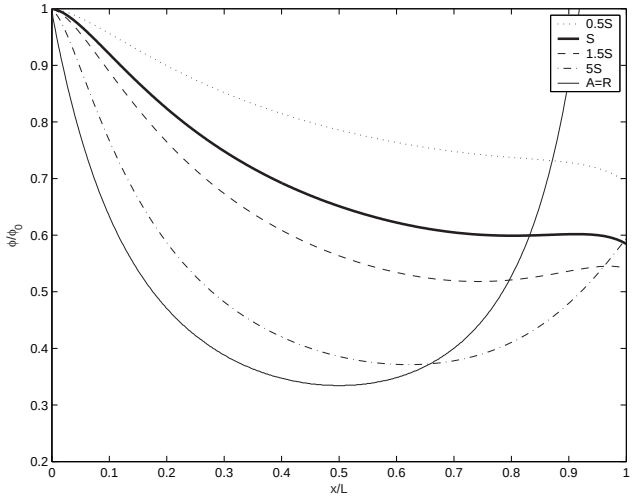

FIGURE 10. The development of flocculation intensity for various levels of the source term

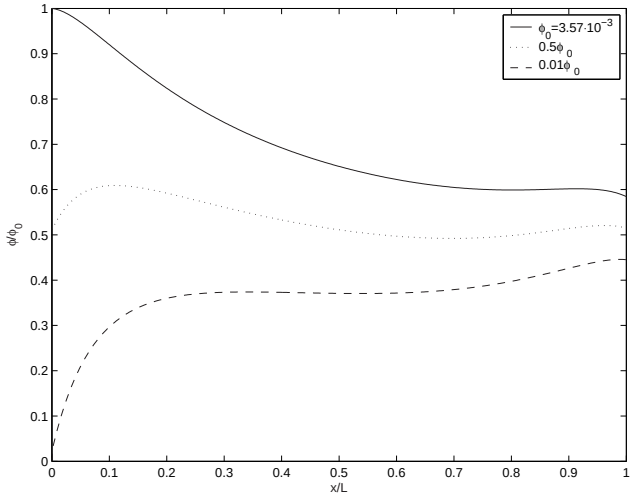

FIGURE 11. Different inlet values for ϕ with FFC-1990

4.1. *Typical Headbox flows*

Increasing the velocity in the contraction will increase the convective part. This will furthermore reduce the time scale, which is important for the flocculation process, cf. Karema *et al.* (2001). The importance of time when increasing the velocity, thus reducing the time scale, is predicted with FFC-1990, cf. Figure 13. The inlet turbulence level, i.e. k_o and ε_0, is kept the same for the

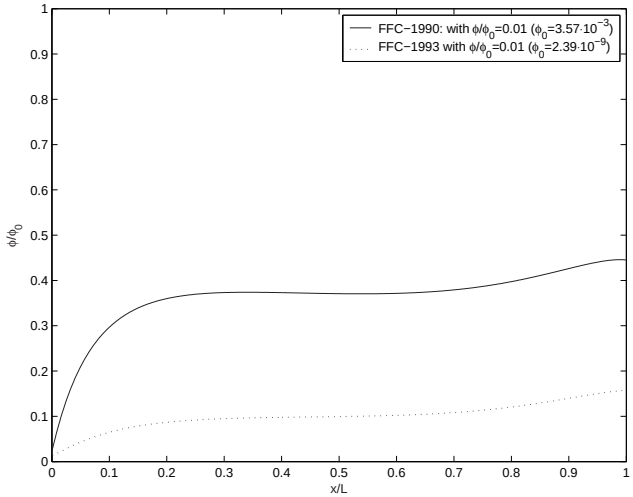

FIGURE 12. Development of the normalized flocculation intensity for inlet values of 0.01 for both FFC-1990 and FFC-1993

different velocities, and this corresponds turbulence intensities 5.45%, 4% and 2.73% with increasing velocity respectively. As can be seen in Figure 13 a), a jet velocity of 33.33 m/s, have the shortest residence time in the contraction and therefore the lowest outlet flocculation intensity value. In Figure 13 b), the normalized flocculation intensity with normalized position along the contraction is shown. The convective dependency or the time scale is also here illustrated giving a lower normalized flocculation intensity gradient with increasing velocity. Note that the flocculation intensity value now will increase from an equilibrium inlet value in contrast with the case earlier, cf. Figure 13, 5 and 7. This is a consequence of the f-function in equation (11) which will strongly activate the aggregation term. The f-function has its maximum value at resonance frequency, ω_0, i.e ratio $\omega/\omega_0 = 1$. The eigenfrequency, ω_0, is a function of fibre dimensions and the stiffness of the fibre, cf. equation (12). Varying the inlet turbulent energy will also change the equilibrium inlet condition, cf. Figure 14. With the two lowest turbulence intensities, i.e. lower activation energy, the flocculation intensity will decrease in the beginning of the contraction and thereafter develop accordingly to the other cases. The highest turbulence intensity will give the lowest outlet flocculation intensity value. The difference in inlet values is larger than the difference of the final outlet values. Different fibre dimensions, e.g. Pine or Birch, will accordingly to the FFC have unique fibre flocculation property. A shorter fibre, e.g. Birch, will have a higher eigenfrequency, and therefore need more turbulent energy in the Kolmogorov scales,cf. equation (4), to be activated for aggregation. The equilibrium flocculation intensity values for different fibre dimensions and for varying turbulence

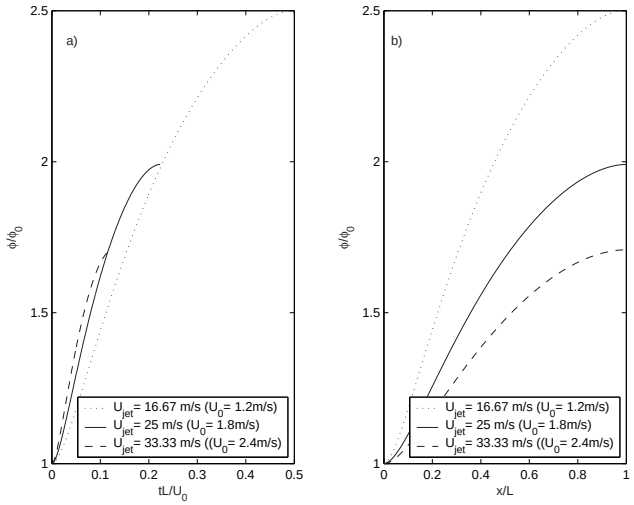

FIGURE 13. a)Development of the normalized flocculation intensity with increasing flow rate for FFC-1990 with residence time. b) The normalized flocculation intensity with normalized position along the contraction

levels with a given dissipation length scale are shown in Figure 15. Starting from a totally homogenous fibre suspension, $\phi_{eq} = 0$, the longer fibre with the lower eigenfrequency will be activated more easily since the Kolmogorov scales have enough energy for activation. Now comparing the case with turbulence intensity of 1% accordingly the longer fibres have a higher level of equilibrium flocculation intensity value. It is known that longer fibre or higher consistency will enhance mechanical flocculation due to a collision mechanism, eg. Mason (1948). The frequency of fibre collisions is increased in both cases. In Figure 15 is this illustrated that the flocculation intensity with a longer fibre is enhanced earlier and it will give higher maximum value of flocculation intensity. If the turbulence intensity is increased further a local maximum is reached. After the maximum the FFC-1990 postulates that the collisions will be less efficient as the typical contact time, $t' \sim k/\varepsilon \sim l_\varepsilon/\sqrt{k_0}$, is shorter than the settling time, t_{fib}, cf. equation (13). The local maxima is present for all the three fibres compared and it is shifted towards higher turbulence intensity value for shorter fibres due to its higher eigenfrequency. High enough turbulence intensity will give almost the same level of equilibrium flocculation intensity for all the three compared fibres. Experimental result by VTT Energy/Metso Paper Inc. provides some results on the development of floc length in CD direction for different outlet jet velocities in a planar contraction for a Birch fibre, cf. Figure 16. As can be seen the floc size for the particular contraction will increase, i.e. reflocculation takes place in the contraction. This was also demonstrated by Karema *et al.* (2001) in a contraction with vanes. In Figure 17 a) the modelled flocculation

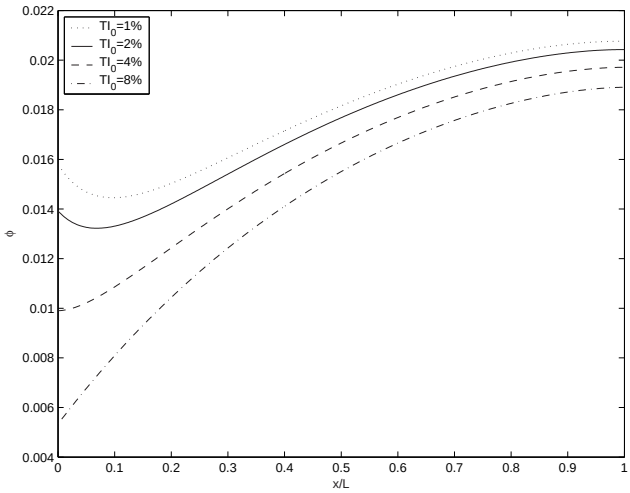

FIGURE 14. Development of the flocculation intensity for different levels of inlet turbulence intensity ($U_0 = 1.8m/s$) for FFC-1990

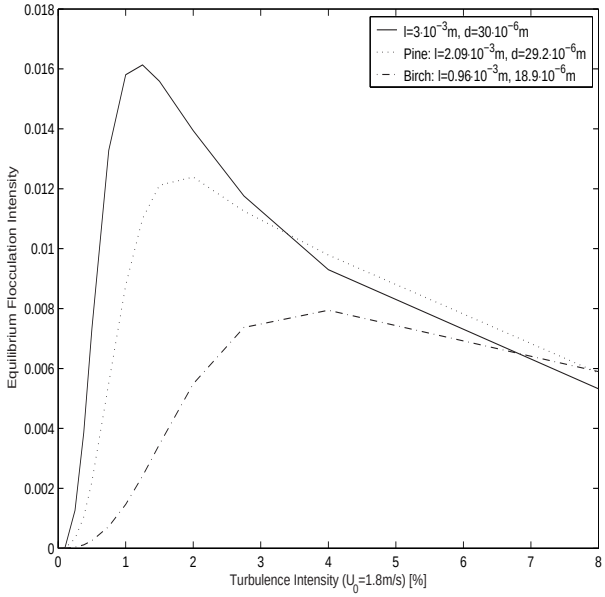

FIGURE 15. Equilibrium flocculation intensity for different fibre dimensions as function of turbulence intensity ($l_e = 10.2 \cdot 10^{-3}m$), Data for Pine and Birch from Karema *et al.* (2001)

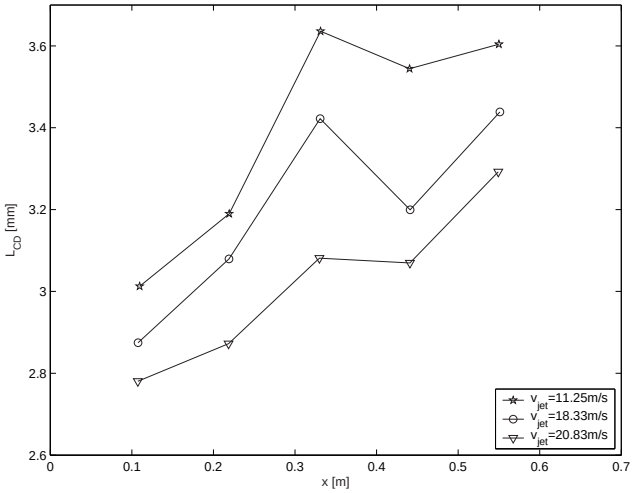

FIGURE 16. Experimental result of CD floc length in a planar contraction by permission from Metso Paper Inc/VTT Energy Jyväskylä, Finland. Birch fibre dimensions: l=0.96mm and d= 18.9μm.

intensity evolution with FFC-1990 for a planar contraction with fibre dimensions, l=3mm and d= 30μm is shown and in b) with fibre dimension for Birch, i.e. l=0.96mm and d= 18.9μm. The modelled result shows different behavior for the case starting from a equilibrium state. The Birch fibre will decrease through out the contraction while the longer fibre will increase in flocculation intensity. The experimental result in Figure 16 indicates that the floc volume will increase for a planar contraction. For the non-equilibrium case, $0.01\phi_0$, both fibre dimension cases predict an increase in flocculation intensity.

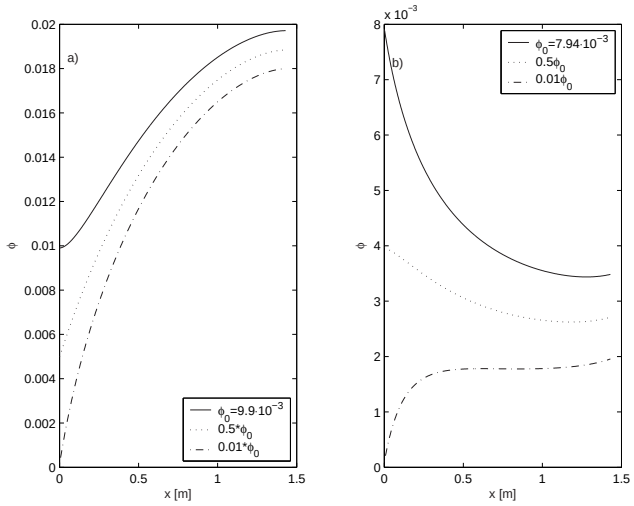

FIGURE 17. a) Modelled flocculation intensity with FFC-1990 in planar contraction with fibre dimensions: l=3mm and d= 30μm. b) Modelled flocculation intensity with FFC-1990 in planar contraction with Birch fibre dimensions: l=0.96mm and d= 18.9μm.

5. Conclusions

The following conclusions can be drawn from this study:

1. Flocculation models proposed by Steen, i.e. FFC-1990 and FFC-1993, is dependent on turbulence quantities, such as k and ε, consequently a careful consideration of turbulence models for a specific flow geometry is of great importance.

2. Results reveal large difference in the magnitude of the flocculation intensity between the two flocculation models. Starting from a equilibrium between aggregation and rupture the later model, FFC-1993, gives a lower magnitude of flocculation intensity.

3. The importance of residence time in the contraction is predicted by means of increasing the flow rate. Result clearly shows that the shortest residence time, i.e. highest flow rate, gives the lowest outlet value of the flocculation intensity. Experimental result by Karema *et al.* (2001) suggests the same behavior.

4. From an equilibrium state of the flocculation intensity, for which the rates of aggregation and rupture are equal, a longer fibre predicts an increase in flocculation intensity in the planar contraction, while a shorter Birch fibre suggests the opposite. On the other hand both fibre types predicts an increase in flocculation intensity from a non-equilibrium state. This trend is also indicated by experimental results.

References

1999-2002 *CFX-5 and CFX-4 User Documentation*. AEA Technology plc.

Andersson, O. 1966 Some observation on fibre suspensions in turbulent motion. *Svensk Papperstidning* **69(2)**, 23–31.

Hourani, M. 1988*a* Fiber flocculation in pulp suspension flow part1: Theoretical model. *Tappi Journal* pp. 115–118.

Hourani, M. 1988*b* Fiber flocculation in pulp suspension flow part2: Experimental results. *Tappi Journal* pp. 186–189.

Hyensjö, M., Hämäläinen, J. P. & Dahlkild, A. 2003 Turbulent dilute fibre suspension flow modelling in a circular pipe enlargement. *89th Annual PAPTAC Meeting, Montreal* .

Karema, H., Salmela, J., Tukiainen, M. & Lepomäki, H. 2001 Prediction of paper formation by fluidisation and reflocculation experiments. *12th Fundamental Research Symposium* pp. 559–589.

Kerekes, R. 1983 Flocculation in decaying turbulence: A literature review. *J. Pulp Paper Sci.* pp. TR86–TR91.

Kuhn, D. & Sullivan, P. 2001 Analysis and measurement of the flocculation intensity of a flowing pulp suspensions. *"2001 Papermakers Confenrence, Cincinatti, OH, USA* .

Launder, B. 1977 Heat and mass transport. In *Topics in Applied Physics: Turbulence, Chapter 6* (ed. P. Bradshaw), , vol. 12.

Mason, S. G. 1948 The flocculation of cellulose fibre suspensions. *Pulp and Paper Magazine of Canada* pp. 99–104.

Mason, S. G. 1954 Fibre motions and flocculation. *Pulp and Paper Magazine of Canada* **55** (13), 96–102.

Moayed, R. 1999 Characterization of fibre suspension flows at papermaking consistencies. PhD thesis, Department of Chemical Engineering and Applied Chemistry, University of Toronto, 1999, Toronto, Canada.

Norman, B., Möller, K., Ek, R. & Duffy, G. 1977 Hydrodynamics of papermaking fibres in water suspension. In *Fibre - Water Interactions in Papermaking: Transactions of the Symposium held at Oxford: September 1977*, , vol. 1(2), pp. 195–249.

Parsheh, M. 2001 Flow in contractions with application to headboxes. PhD thesis, Royal Institute of Technology, Stockholm, Sweden.

Plikas, A., Kuhn, D. & Sullivan, P. 2000 A numerical model of fibre suspensions in a grid generated turbulent flow. In *ASME 2000 Fluids Engineering Division Summer Meeting: Proceedings of ASME FEDSM'00 held in Boston, Massachusetts, USA*, pp. 991–996.

Rodi, W. 1993 *Turbulence Models and Their Application in Hydraulics A State-of-the-art review*, 3rd edn. IAHR-AIRH, A.A.Balkema, Rotterdam.

Steen, M. 1990 Modelling fibre flocculation in turbulent flow; a numerical study. *TAPPI Engineering Conference, Seattle, USA* pp. 475–486.

Steen, M. 1993 On turbulence and flocculation in fibre suspensions. *Institue of Paper Science and Technology, Atlanta, Georgia USA* .

Wahren, D. 1967 Proposed definitions of some basic papermaking terms. *Sv. Papperstidning* **70(21)**, 725.

Paper 3

3

Modelling a Turbulent Dilute Fibre Suspension in a Planar Contraction: Effect of Vane Types, Vane Position and Wall Boundary Layer on Fibre Orientation Distribution

By Marko Hyensjö[1,4], Paul Krochak[2], James Olson[2], Jari Hämäläinen[3], Anders Dahlkild[4]

[1]Metso Paper Karlstad AB, P.O. Box 1014, SE-651 15 Karlstad, Sweden
[2] The Pulp and Paper Centre, Dept. of Mechanical Engineering, University of British Columbia, 2324 Main Mall Vancouver BC Canada V6T 1Z4, krochak@interchange.ubc.ca, olson@mech.ubc.ca
[3]Department of Applied Physics, University of Kuopio, P.O.Box 1627, FIN-70211 Kuopio, Finland, Jari.Hamalainen@uku.fi
[4]FaxenLaboratoriet, Royal Institute of Technology KTH, SE-100 44 Stockholm, Sweden, ad@mech.kth.se

In *Proceedings of the 5th International Conference on Multiphase Flow, ICMF'04*, Yokohama, Japan

A model of the effect of turbulence generating vanes and its location in a planar contraction for predicting fibre orientation distribution is proposed. Simultaneously with CFD simulations and with experimental data, the non-dimensional rotational dispersion coefficient has been determined for the extended 1D headbox model. Furthermore the behavior of turbulence generating vanes types, i.e. blunt and tapered, and the location of such has been studied. For different streamlines in the contracting channel, the one dimensional fibre orientation distribution model is solved, and the fibre orientation distribution is studied along streamlines near the vane wall and vane tip and further away. The model reveals the effect of the vane tip and the wall boundary layer on fibre orientation distribution. The boundary layer will for both in the plane of paper and in the plane of contraction wider the fibre orientation distributions, i.e the fibres will be less oriented. For the outlet profile of the contraction the fibre orientation distribution will be more effected by the blunt vane tip than the tapered vane tip. The model is validated with experimental results in literature and a good qualitatively agreement was archived.

---

1. Introduction

In papermaking a cellulose fibre suspension in water is formed and dried into a continuous paper web. The formation of this web in a paper machine begins

in the wet end or in the forming section. In the forming section the dilute fibre suspension is accelerated by passing through a contracting duct and evenly spread out as a jet onto a moving fabric or into a gap of two moving fabrics. The jet can be about 10mm thick and 10m wide. The formation, i.e. the small scale basis weight variation, is dependent on the state of fibre suspension in this forming section. To ensure a good formation the fibres must be evenly dispersed in the suspension. The paper strength properties in machine direction and cross-machine direction as well as in thickness direction (i.e. z-direction) are important for runnability and dimensional stability of the paper sheet in copying and printing machines. The strength properties are determined by chemicals, fibre type and preparation, but also largely by anisotropy of fibre orientation distribution. Many of the final paper properties is based upon the state of the fibre suspension in the early stage of the process, e.g. Norman & Söderberg (2001). As the jet hits the moving fabric the state or the history of this jet is essential. The jet is formed in the so called headbox. The headbox ensures that the jet leaves with a specific state depending on the type of paper web to be produced. The interaction between this jet and the moving fabric(s) is a main feature for achieving the desired final result. For example in high speed printing it is desirable to have high tensile strength in the direction of the paper feed. For other application such as sack paper it is required to have a uniform distribution and orientation distribution of the fibres. The state of the jet can be modified in various way, one way is to vary the contraction ratio, i.e. the ratio between the inlet height and outlet height of the contracting channel. By increasing the contraction ratio it is known that it significantly increases the fibre alignment, e.g. Ullmar (1997), Ullmar (1998) and Zhang (1998), and this can essentially change the final paper properties, e.g. Nordström & Norman (1994) and Söderberg & Kiviranta (2003). Other ways is to insert vanes into the contracting channel of the headbox. These vanes depending on type and length generate turbulence and this can disperse and disorient fibres, i.e result in a more uniform sheet by means of final strength of the paper. The effect of the vane tip location on fibre mixing was experimentally studied by Lloyd & Norman (1998). This was done by dying a layer of pulp fibres blue, passing them through a hydraulic headbox and then scanning a finished sheet of paper for the variation of blue content. Their results showed that different vane locations can in fact lead to different levels of mixing. Conventional headboxes use also a slice bar near the exit to control the cross machine direction (CD) basis weight profile. Simultaneously it also affects to fibre orientation angle. When modern headboxes of today utilizes dilution water to control the CD basis weight profile, the slice bar can be used just to adjust fibre orientation angle profile. Unfortunately very little is known on neither the effect of turbulence vanes, nor on the effect of a slice bar or headbox geometries, all of which can have a significant effect on fibre orientation anisotropy.

The main purpose of this study is to use numerical modelling to evaluate the effect of turbulence generating vanes and wall boundary on fibre orientation distribution in a planar contraction. In this paper an approach to use the

CFD modelling as an input for the extended one dimensional headbox model is illustrated. Earlier modelling studies have neglected the influence of turbulence in an accelerated fluid flow, e.g. Zhang (1998), Olson (2002) and Akbar & Altan (1992). The rotational dispersion coefficient, in the extended one dimensional headbox model, will be determined with CFD analysis, and validated with experimental data presented in the work by Ullmar (1998). The rotational dispersion coefficient has been related to turbulence quantities, cf. Olson & Kerekes (1998), Olson (2001) and Krushkal & Gallily (1988). The relationship is based on Kolmogoroffs local isotropic hypothesis for very small eddies of the turbulence spectrum, cf. Equation (4). When the rotational dispersion coefficient is determined, arbitrary geometries with or without vanes is studied. In the experimental work by Asplund & Norman (2003), the fibre orientation anisotropy in a jet after a planar contraction with vanes was regarded. Result from this study has been used as a validation and comparison of the extended one dimensional headbox model in this paper.

2. Modelling Approach

In tracking particles in any flow, one of two approaches can be used. A Lagrangian model is based on solving the equations of motion for an individual particle in a given flow field. The fibres orientation and position distribution are then determined from the statistics of a collective ensemble of trajectories. An Eulerian model is based on determining a probability distribution function (PDF) of the fibre orientation and position in a fixed geometric space. In application to turbulent flows, two components must be considered: a mean component and a fluctuating component. The Eulerian PDF is determined by solving a convection-dispersion equation where the mean component of the flow transports the fibres position and orientation distribution, while the fluctuating component disperses fibres against the gradient of the position and orientation distribution. The major advantage to the Eulerian model is that it requires far less computation time, which is often a practical advantage for many engineering applications, and has the potential to account for the effect of increasing particle concentration. Firstly in this section the fluid flow CFD modelling setup will be described and then the theory of the extended one dimensional headbox model.

2.1. *CFD simulation*

The Computational Fluid Dynamics calculations for the fluid flow has been carried out with the commercial CFD code, CFX5, ver. 5.6. The geometrical outline in this study has experimentally been studied by Parsheh (2001). The geometry consists of a planar contraction with one vane in the centreline of the contraction. Two of the four different vane tips in the work by Parsheh (2001) have been studied here, i.e. the blunt and the tapered one. All the simulations were turbulent, and the turbulent fluid flow was modelled with the omega-Reynolds Stress Model turbulence model, with the default values of the

constants provided in the CFD code, cf. CFX (1999-2002). Different turbulence models were examined by Parsheh (2001), and the isotropic k-ε turbulence model failed to describe the turbulence quantities in a planar contraction, while LLR-Reynolds Stress Model and Algebraic Reynolds Stress models did perform better. This motivates the use of the Omega-Reynolds Stress Model instead of an isotropic model. Boundary conditions for the inlet was set to a specified velocity corresponding to the same flow rate as in the work by Parsheh (2001), i.e equal to a Reynolds number of 50000. The turbulence quantities at the inlet was set to specified turbulence intensity of 3.7% and autocompute length scale, c.f. CFX (1999-2002). The turbulence intensity, TI, is defined as:

$$TI = \sqrt{\frac{\overline{u^2}}{U^2}} \tag{1}$$

This value is an estimate from measurements by Parsheh (2001) for a slightly lower Re number for the same specific turbulence grid generator. The wall boundary was resolved with Y^+ values between 2-3 for the first node closest to the wall. A symmetrical boundary condition was set for the centerline of the geometry.

2.2. *The Extended One Dimensional Headbox Model*

The convection-dispersion equation describing the evolution of fibre orientation in a one dimensional headbox, as derived by Olson *et al.* (2004), is here extended to be valid for an arbitrary streamline. The extended one dimensional headbox model is then given for a coordinate system, s, following a streamline as:

$$\frac{\partial \Psi}{\partial t} + U_s \frac{\partial \Psi}{\partial s} = D_p \frac{\partial^2 \Psi}{\partial \phi^2} - \frac{\partial (\dot{\phi} \Psi)}{\partial \phi} \tag{2}$$

where s is defined as the square root of the sum of the squared values of the plane coordinate variables, x and y resp., and U_s is the tangential average velocity along the streamline. Note that even though we are following a streamline this is still a Eulerian approach since we are not following individual fibres. D_p is the rotational dispersion coefficient and ϕ is the projected angle in the plane of contraction. The first term is the time derivative of the fibre orientation distribution. Equation (2) is simplified by assuming steady flow, and made dimensionless with the scaled variables $\overline{s} = \frac{s}{L_s}$ and $\overline{U_s} = \frac{U_s}{U_0}$, where L_s is the length of the streamline considered. This gives the following expression for fibre orientation in the plane of contraction along a streamline:

$$\overline{U_s} \frac{\partial \Psi}{\partial \overline{s}} = \overline{D_p} \frac{\partial^2 \Psi}{\partial \phi^2} - \frac{\partial}{\partial \phi} (\dot{\phi} \Psi) \tag{3}$$

The dimensionless rotational dispersion coefficient, $\overline{D_p}$, is expressed in analogy with, cf. Olson & Kerekes (1998), Olson (2001) and Krushkal & Gallily (1988). This relationship is based on Kolmogoroffs local isotropic hypothesis for very

small eddies of the turbulence spectrum:

$$\overline{D_p} = const \frac{L_s}{U_0} (\frac{\varepsilon}{\upsilon})^{\frac{1}{2}} \tag{4}$$

where, L_s, is the streamline length and U_0, is the inlet mean velocity. In previous studies, e.g. in Olson *et al.* (2004), $\overline{D_p}$ was considered to be constant and that in this study ε is a function of position through the duct and is estimated from CFD modelling. In Equation(3) the non-dimensional rotational velocity in the plane of contraction is given by Olson & Kerekes (1998) for a straight, rigid, infinitely thin, inertialess fibre to be:

$$\dot{\phi} = -\frac{\partial \overline{U}}{\partial \overline{x}} \sin 2\phi + \frac{\partial \overline{V}}{\partial \overline{x}} \cos^2 \phi - \frac{\partial \overline{U}}{\partial \overline{y}} \sin^2 \phi \tag{5}$$

The dimensionless expression for fibre orientation in the plane of the paper, γ, is identical to Equation (3) with the exception that rotational velocity is defined, cf. Olson (2001), as:

$$\dot{\gamma} = -\frac{1}{2} \frac{\partial \overline{U_s}}{\partial \overline{s}} \sin 2\gamma \tag{6}$$

which is here expressed in the coordinate system following a streamline. It has been assumed that fibres entering the headbox are randomly oriented. This agrees well with the experimental findings of Zhang (2001) very near the inlet, hence the initial condition expressed for ϕ is:

$$\Psi(0, \phi) = \frac{1}{\pi} \tag{7}$$

The boundary condition for Equation (3) is set to be periodic with respect to ϕ or γ, meaning that the gradient of Ψ is set to be equal at the boundaries $\pm\pi/2$ and also the value of Ψ is equal. The one dimensional headbox model and this extended one considers only the mean translation of the fibres along streamlines. Translational dispersion, both in the direction of the flow and perpendicular to the flow direction are neglected. Equation (3) has been modelled with MatLab ver. 12 by the Gauss-Siedel iterative method. For the finite differences the fully implicit formulation was used with a second order approximation.

3. Model Validation

3.1. *Fluid Flow*

In Figure 1, (a) and (c), the mean velocity value divided by undisturbed velocity, U_e, for different positions in the wake after the two different vane tips is presented for both experimental data of Parsheh (2001) and CFD simulations. Furthermore in Figure 1, (b) and (d), describes the fluctuating streamwise velocity component, u. The results for the tapered vane is at a position 1 mm downstream from the tip in figure 1, (a) and (b) and 6 mm for the blunt vane. Figures (c) and (d) is at 151 mm downstream from the vane tip for both of the vane types Both vanes have a thickness of 5.5mm and the tapering starts

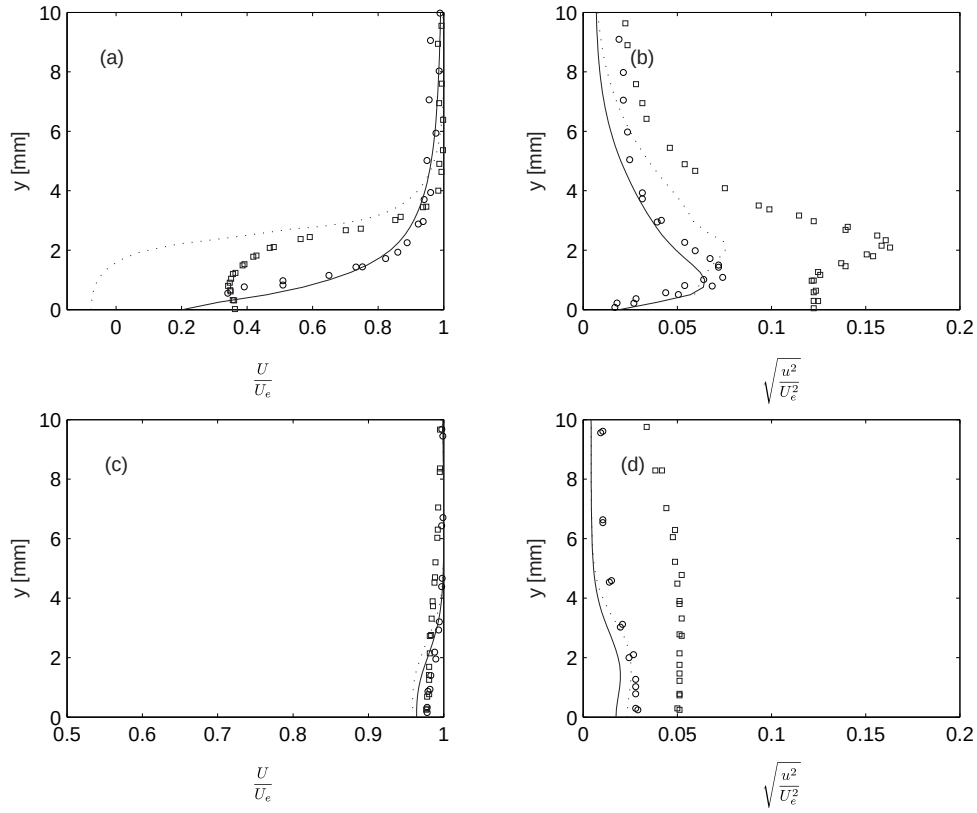

FIGURE 1. Validation of CFD simulations against experimental data of Parsheh (2001). The experimental data for tapered vane tip is denoted circles and the blunt vane tip with squares and simulations is denoted by solid and dotted line for tapered and blunt vane tip respectively.

35mm back from the tip. The centerline is located at y=0. As can seen from the results the tapered vane shows a good agreement with experimental data.

For the blunt vane tip no recirculation mean velocity was recorded in the experiment, which was seen in simulation. Furthermore the turbulence was underestimated according to experiments. This can come from the fact that instabilities occur for this size of blunt vane tip, 5.5 mm, and this can give rise to enhanced turbulence dispersion. A vortex shedding effect can explain the behavior of this effect. In simulation restriction was made due to the symmetrical boundary condition. These simulations were made with air as fluid. The same approach was used for simulations made with water as described above, at Re number of

50000. The wall boundary was resolved and once again so that Y^+ of 2-3 was achieved.

3.2. *Fibre Orientation Distribution*

In previous work, a convection-dispersion model of fibre orientation in a one dimensional headbox was derived and numerically studied by Olson *et al.* (2004). The model accounts for a constant value, 2.5, of the dimensionless rotational dispersion coefficient and it was shown to agree well with the independent findings of Ullmar (1998). The constant in the dimensionless rotational dispersion coefficient presented in equation (4) has been determined and validated with the results presented by Ullmar (1998). This resulted in the following correlation:

$$\overline{D_p} = 6.57 \times 10^{-2} \frac{L_s}{U_0} (\frac{\varepsilon}{\upsilon})^{\frac{1}{2}} \tag{8}$$

This result is about 5.5 times smaller than the proposed value by Olson (2001). In the work by Olson (2001) this expression was derived for isotropic homogeneous turbulence, which is not the case here.

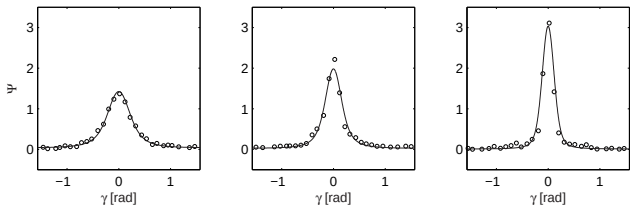

FIGURE 2. Predicted and measured, Ullmar (1998), fibre orientation distributions for contraction ratios of 16.7, 25, 50.

In Figure 2 results for different contraction ratios of 16.7, 25 and 50, of the proposed correlation in equation (8) compared to experimental data of Ullmar (1998) can be seen. These results are from the outlet in the centerline of the contraction and made in the plane of paper, i.e. γ. This suggest a good agreement between the predicted and measured data for the different contraction ratios. This also demonstrates the enhanced alignment of fibres in a increased contraction ratio. The dimensionless rotational turbulent dispersion in Equation (8) is used for both γ and ϕ in this paper.

Example of development of the computed fibre orientation distribution along a contraction with a contraction ratio of 50, can be seen in Figure 3. There is a trend for increased orientation of fibres at the end of the contraction which seems to be a reasonable result, since the velocity gradient is almost exponentially increasing. Even the dimensionless rotational dispersion coefficient is

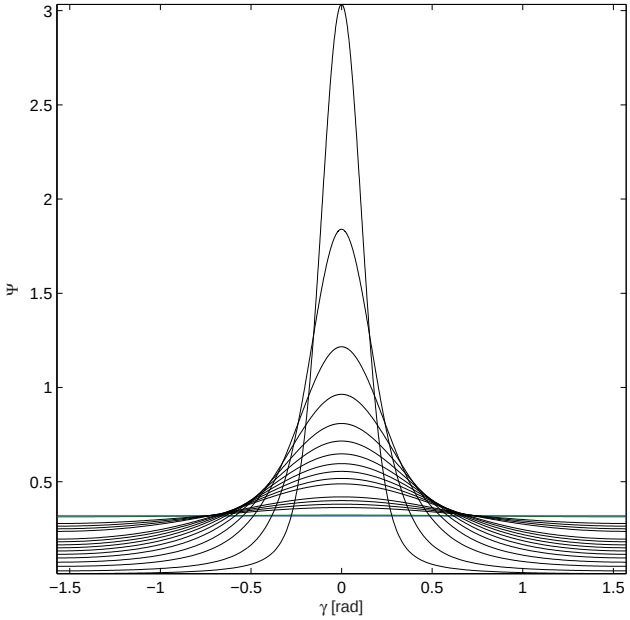

FIGURE 3. Development of fibre orientation distribution along the centerline streamline for contraction ratio of 50.

increased in the end of the contraction, cf. Figure 4. This is due to the increase in turbulent dissipation rate in such fluid flow. Furthermore there seems to be a constant part in the beginning of the contraction. Also, the higher the contraction ratio is the lower is this constant part and it accelerates in the end of the contraction. The final outlet value is highest for the highest contraction ratio. The constant value representing the solid line was assumed by Olson *et al.* (2004), and the CFD calculations shows that this is significantly non linear through the duct.

4. Results

Since the fibre orientation distributions for γ are nearly Gaussian distributions, cf. Figure 3, the degree of fibres not being oriented towards γ=0 is represented by the standard deviation $\sigma(\gamma)$:

$$\sigma_\gamma^2(x,y) = \int_{-\frac{\pi}{2}}^{+\frac{\pi}{2}} \gamma^2 \Psi(\gamma,x,y) d\gamma \tag{9}$$

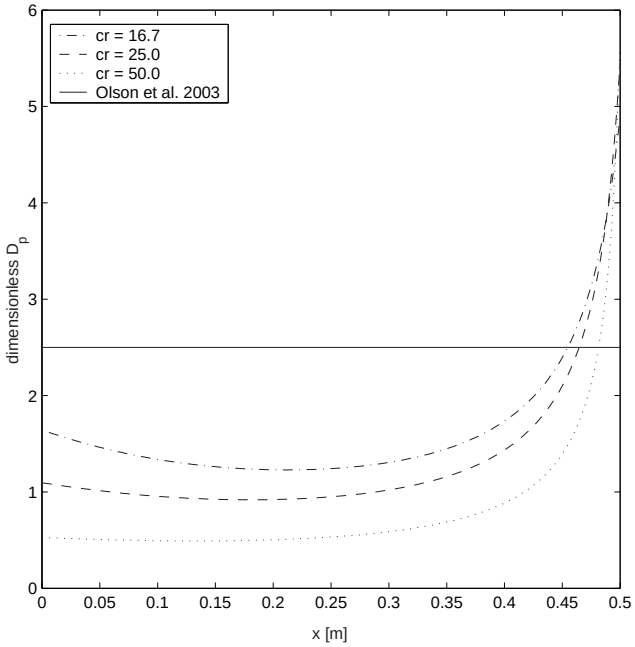

FIGURE 4. Dimensionless rotational dispersion coefficient along the centerline for different contraction ratios of 16.7, 25, 50.

$\Psi(\gamma, x, y)$ is here the normalized distribution function for γ on the interval $-\pi/2 \leq \gamma \leq +\pi/2$. For ϕ we may make an analogous definition:

$$\sigma_\phi^2(x,y) = \int_{-\frac{\pi}{2}}^{+\frac{\pi}{2}} (\phi - \phi_m)^2 \Psi(\phi, x, y) d\phi \tag{10}$$

where $\Psi(\phi, x, y)$ is the distribution function for ϕ. One may observe that, although the mean value of ϕ taken over a complete cross section of the channel is zero, this is not necessary the case for the local mean value $\phi_m(x, y)$, cf. Figure 5, 6 and 7.

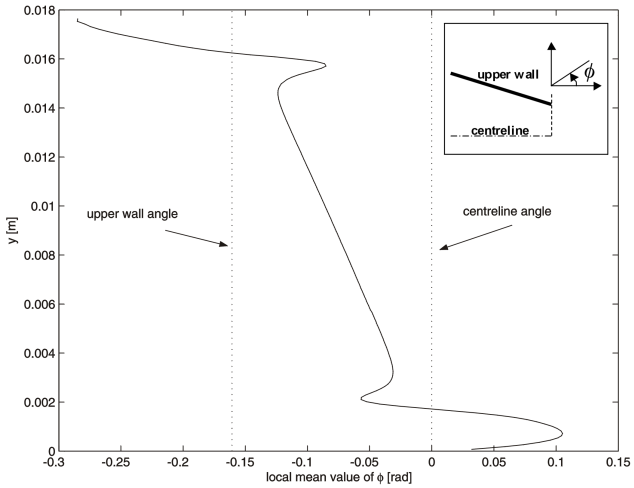

FIGURE 5. Outlet profile of the local mean value of ϕ for a tapered vane at vane position -80 mm from the outlet.

Figure 5 shows the local mean value, ϕ_m, across the outlet section, from the centreline and to the upper wall. The overall trend at the outlet is a mean orientation basically along the local flow direction, gradually approaching the inclination of the upper wall for increasing distance from the centreline. Deviations from this trend appear in the shear layers of the wake and the wall, where fibres close to the wall have a mean angle less than the upper wall it self and fibres in the lower part of the wake have a positive mean angle. In Figure 6 the local mean value of ϕ is shown as a contour plot over the whole contraction. The mean value at the inlet is zero as a consequence of the inlet conditions, cf. Equation 7. Also the boundary layer effect can be noted, for the upper wall with negative values as shown in Figure 6 and for the vane wall boundary with positive values, meaning that the fibres heads are pointing upwards. The effect of the tapered vane tip will decrease the mean value locally as can be seen in Figure 6 and in more detail in Figure 7, as a result of deflection of the streamlines in the area around the vane tip. The value of σ_γ and σ_ϕ along different streamlines have been converted into contour plots, cf. Figures 8 and 9. A smaller standard deviation value means a larger degree of orientation towards the mean value of the fibres and vice versa. In Figures 8 and 9 the top two figures represent a contraction with no vane, and the middle figures and the bottom figures represent the tapered and blunt vane tips respectively. The left column represents the degree of orientation in the plane of paper and the right column the degree of orientation in the plane of the contraction. In Figure 8 one can clearly see how the boundary layers of the wall and the vane causes the degree of orientation towards γ=0, to decrease. This result was

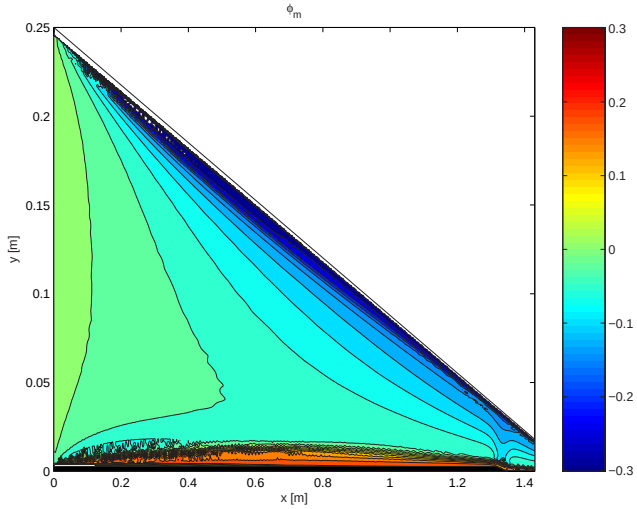

FIGURE 6. Overview contour plot of the local mean value of ϕ for a tapered vane at vane position -80 mm from the outlet.

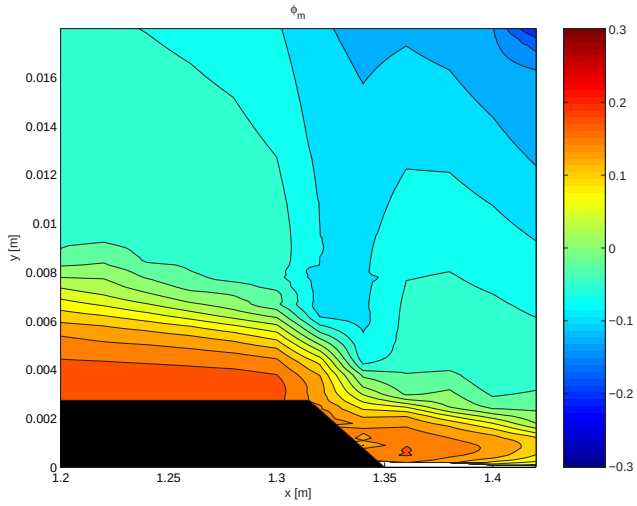

FIGURE 7. Close up contour plot of the local mean value of ϕ in the vicinity of a tapered vane tip at a position -80 mm from the outlet.

experimentally shown by Asplund & Norman (2003). From this figure no clear difference between the vane tips is obvious.

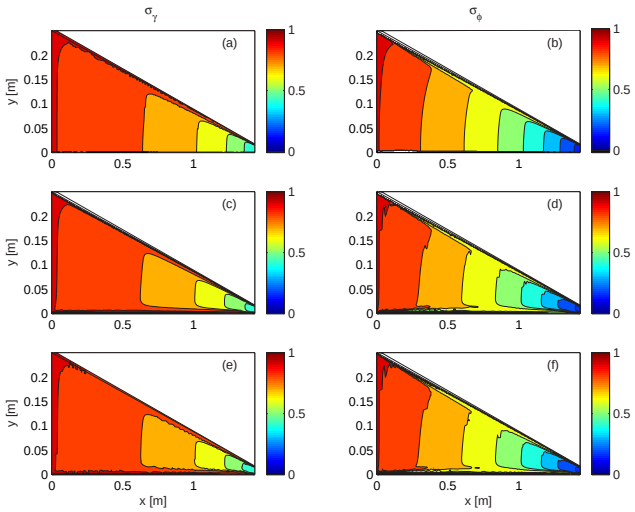

FIGURE 8. Overview contour plots for three different cases, (a) and (b); no vanes, (c) and (d); tapered vane tip, (e) and (f); blunt vane tip.

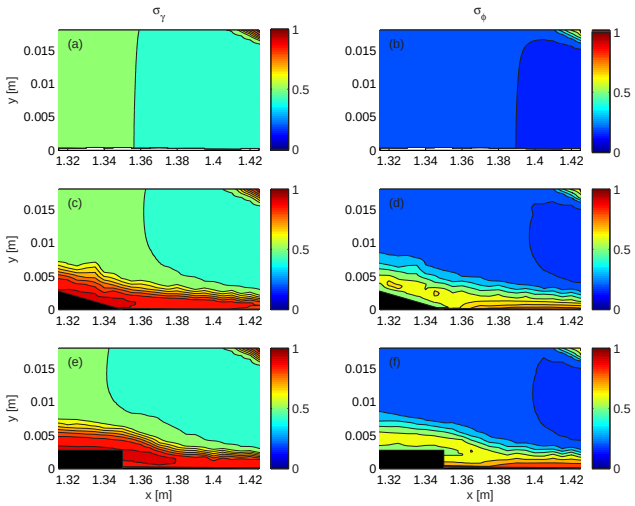

FIGURE 9. Close up contour plots near the vane tip and downstream to the slice opening for the three different cases, (a) and (b); no vanes, (c) and (d); tapered vane tip, (e) and (f); blunt vane tip.

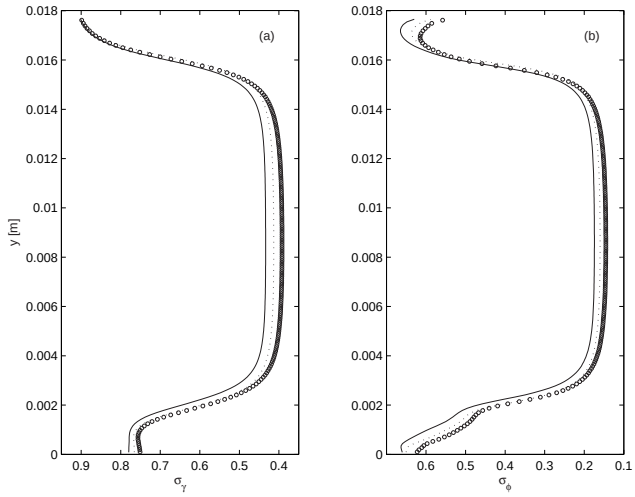

FIGURE 10. Standard deviation outlet profiles for γ, (a), and ϕ, (b), at different flow rates, denoted with a dotted line for Q_{ref}, circles for a flow rate $0.7Q_{ref}$ and a solid line for a flow rate $1.3Q_{ref}$, for a blunt vane tip at a position -230mm from the outlet.

A close-up contour plot in the vicinity of the vane tip is presented in Figure 9. Here the height of the figure is the outlet opening of the contraction. A clear influence of the respective vane tip is observed downstream, where the blunt vane tip has a wider effect. In Figure 10 the influence of different flow rates is illustrated at the outlet of the contraction for a blunt vane tip. The flow rate was varied ±30% from the original reference value, Q_{ref} (corresponds to Re=50000). Note that the x-axis has been reversed to illustrate the effect of the degree of orientation towards the mean value, rather than the spreading around the mean value more clearly. Clearly the lowest flow rate will give a slightly higher degree of orientation towards the mean value of fibres in the undisturbed region and in the wake of the vane tip in the vicinity of the centreline. The overall increase in turbulence level as the flow rate increases would explain the decrease in the the degree of orientation towards the mean value in the wake from the vane tip and in the undisturbed region for both γ and ϕ, cf. Figure 10. The effect of wall boundary layer on the degree of orientation towards the mean value can also be seen in Figure 10. Asplund & Norman (2003) showed a clear trend toward a lower anisotropy for higher flow velocities close to the wall for γ, caused maybe due to an increased overall turbulence level. In their study a wide flow range were studied from velocities about 2 m/s to over 10 m/s. In this study the mean flow velocity is about 0.9 m/s ±30%. Figure 10 reveal no clear difference for increasing flow rates in the immediate region

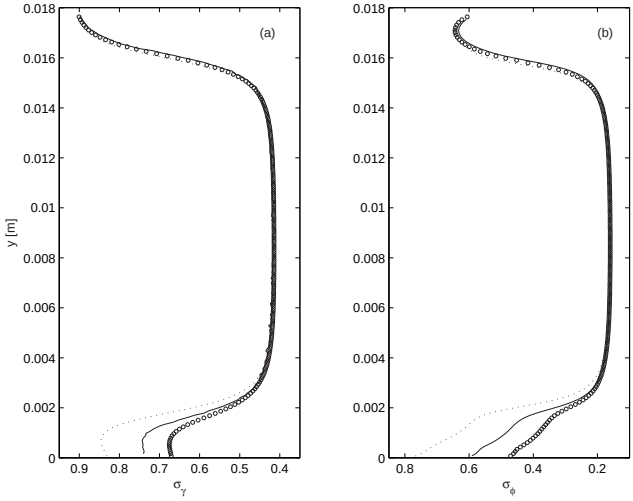

FIGURE 11. Standard deviation outlet profiles for γ (a) and ϕ (b), at different vane positions: -80 (..), -230 (-) and -380 (o) mm from the outlet, for a tapered vane tip.

closest to the wall for the angle in the plane of the paper, γ. The results for σ_γ for different flow rates deviates from each other approximately 3mm from the upper wall and further away to the undisturbed region. The value of standard deviation for γ of about 0.9, indicates that the fibres have almost no preferred direction closest to the wall. Note that the fibres in the simulations has no extension while in the experimental result by Asplund & Norman (2003), 3mm long nylon fibres were used.

For the angle in the plane of the contraction, ϕ, there seems to be differences for the result of σ_ϕ between the flow rates close to the wall. The lowest flow rate will give more degree of orientation towards the mean value. There is also a trend for decreasing of σ_ϕ in the immediate region of the wall. This can be explained by that turbulence will decrease the degree of orientation towards the mean value in the outer part of the boundary layer and in the near wall region the velocity gradient (increase of $\partial u/\partial y$) causes σ_ϕ to decrease and also the fibres to orient towards a smaller negative mean angle, cf. Equation 3 and Figure 5.

The effect of vane position is presented in Figure 11. The closer the vane is to the outlet the larger is the effect on the σ_ϕ. This trend is similar to experimental data for the fibre orientation anisotropy, cf. Asplund & Norman (2003). In their work for a thick, blunt vane tip at a mean velocity of 5 m/s, the undisturbed region was vanishing as the vane tip was moved closer to the

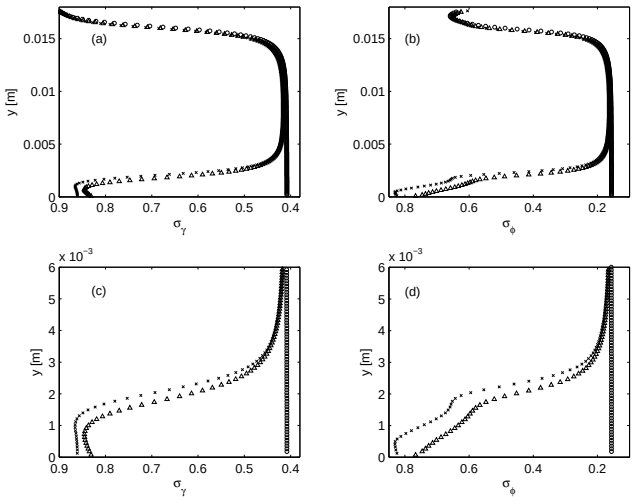

FIGURE 12. Overview, (a) and (b), and close-up, (c) and (d), outlet profiles for different vanes, blunt (x) and tapered (triangle) and no vane (circle), at vane position: -80 mm from the outlet.

outlet. The clear difference of σ_γ and σ_ϕ when comparing the different vane tips at a fixed position and flow rate is shown in Figure 12. The wider wake from a blunt tip compared to the tapered vane tip, results in a lower degree of orientation towards the mean value, i.e. in correspondence to experimental data for γ, cf. Asplund & Norman (2003).

5. Conclusions

A model for predicting fibre orientation distribution in a headbox contraction with a turbulent generating vane is proposed and the effect of vane location and shape. The non-dimensional rotational Dispersion coefficient for the extended 1D headbox model has been determined with CFD simulations together with available experimental data. The behavior of vanes types, i.e. blunt and tapered, and the location of such has been modelled. For different streamlines in the contracting channel, the one dimensional fibre orientation distribution is solved, leading to that the fibre orientation distribution could be studied for streamlines near the vane wall and vane tip and further away. The model reveals the effect of the vane tip and the wall boundary layer on fibre orientation distribution. Following findings in this study could be concluded:

1. The magnitude of the rotational dispersion coefficient is determined for a contracting channel to be according to Equation 8.

2. A method to solve Equation 4 together with CFD, along different streamlines

and with a rotational dispersion coefficient dependent on turbulence quantities, is presented. This will reveal effects of wall boundaries and wakes on fibre orientation distribution in a two-dimensional frame.

3. Different experimental results reported in the literature, i.e. Asplund & Norman (2003), was compared with this modelling approach and a good qualitatively agreement was archived.

6. Acknowledgement

Marko Hyensjö would like to acknowledge the financial support from Metso Paper Inc. and also the Swedish Association of Pulp and Paper Engineers and the Gustav och Emrick Hellströms Stipendiefond for contribution of travelling expenses. Furthermore he would like to thank the Pulp and Paper Centre at UBC for giving him the opportunity to spend three months during summer 2003. Paul Krochak and James Olson would like to acknowledge the financial support of the Natural Science and Engineering Research of Council of Canada.

References

1999-2002 *CFX-5 and CFX-4 User Documentation*. AEA Technology plc.

Akbar, S. & Altan, C. 1992 On the solution of the fibre orientation in two-dimensional homogeneous flows. *Polymer Eng. Sci.* .

Asplund, G. & Norman, B. 2003 Fibre orientation anisotropy profile over the thickness of a headbox jet. *89th Annual PAPTAC Meeting, Montreal* .

Krushkal, E. M. & Gallily, I. 1988 On the orientation distribution function of non-sperical aerosol particles in a general shear flow - ii. the turbulent case. *Journal of Aerosol Science* **19**, 197–211.

Lloyd, M. D. & Norman, B. 1998 Layer mixing during three-layer stratified formning: The role of vane lenght and mix-wire speed difference. *Tappi Journal* pp. 194–201.

Nordström, B. & Norman, B. 1994 Influence on sheet anisotropy, formation, z-toughness and tensile stiffness of reduced feed area to a headbox nozzle. *Nordic Pulp and Paper Research Journal* **1(9)**, 53–59.

Norman, B. & Söderberg, D. 2001 Overview of forming literature, 1990-2000. *Trans. 12th Fundamental Research Symposium, Oxford* **1**, 431–558.

Olson, J. A. 2001 The motion of fibres in turbulent flow, stochastic simulation of isotropic homogeneous turbulence. *International Journal of Multiphase Flow* **27**, 2083–2103.

Olson, J. A. 2002 Analytical estimate of the fibre orientation distribution in a headbox flow. *Nordic Pulp and Paper Research Journal* **3 (17)**, 302–306.

Olson, J. A., Frigaard, I., Chan, C. & Hämäläinen, J. P. 2004 Modelling a turbulent fibre suspension flowing in a planar contraction: The one-dimensional headbox. *International Journal of Multiphase Flow* **30**, 51–66.

Olson, J. A. & Kerekes, R. J. 1998 The motion of fibres in turbulent flow. *Journal of Fluid Mechanics* **377**, 47–64.

Parsheh, M. 2001 Flow in contractions with application to headboxes. PhD thesis, Royal Institute of Technology, Stockholm, Sweden.

Söderberg, D. & Kiviranta, A. 2003 Improvement of base-ply formation through headbox modification. *89th Annual PAPTAC Meeting, Montreal* .

Ullmar, M. 1997 Observations of fibre orientation in a headbox model at low consistency. *Tappi proceedings, Engineering and Papermakers Conference* p. 865.

Ullmar, M. 1998 On fibre alignment mechanisms in a headbox nozzle. *Licentiate Thesis, Royal Institute of Technology, Stockholm, Sweden* .

Zhang, X. 1998 Fibre orientation in a headbox. *Masters Thesis, The University of British Columbia, Vancouver, Canada* .